Comunicações Geológicas

Versão online: https://www.lneg.pt/wp-content/uploads/2020/07/Volume_107_III.pdf

Comunicações Geológicas (2020) 107, Especial III, 111-132
ISSN: 0873-948X; **e-ISSN:** 1647-581X

Geological correlation of Neves-Corvo Mine and Pomarão Antiform sequences (Iberian Pyrite Belt, Portugal)

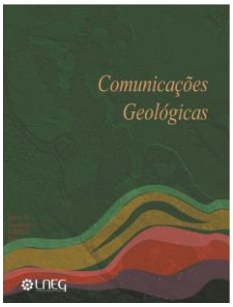

Correlação geológica das sequências da Mina de Neves-Corvo e do Pomarão (Faixa Piritosa Ibérica, Portugal)

L. Albardeiro[1*], J. X. Matos[1], M. Mendes[2], R. Solá[3], Z. Pereira[2], I. Morais[1], R. Salgueiro[3], N. Pacheco[4], V. Araújo[4], J. T. Oliveira[3]

Artigo original
Original article

© 2020 LNEG – Laboratório Nacional de Energia e Geologia IP

Abstract: A geological correlation between Neves-Corvo (NC) and Pomarão antiforms is attempted. These regional scale major sequences are easily correlated but, at local scale, facies and age differences stand out. Stratigraphy includes: i) the Phyllite-Quartzite Group with identical paleogeography setting and similar late Famennian ages for uppermost levels (LL to LN miospore biozones in Pomarão and NC respectively). ii) the Volcano-Sedimentary Complex shows some discrepancy concerning the age distribution of the felsic volcanic rocks (ca. 356-330 for Pomarão and ca. 365-346 Ma for all NC area) while sediments range from mid-Famennian to late Visean age (VH to NM Miospore Biozone for NC). iii); the Baixo Alentejo Flysch Group (late Visean NM Miospore Biozone onwards in NC), covering the previous sequences and being slightly older than the uppermost volcanic rocks of Pomarão. The correlation between these two structures is supported by geology and isotopic/biozone ages and favours exploration scenarios in both regions.

Keywords: Neves-Corvo, Pomarão, stratigraphy, geochronology, Iberian Pyrite Belt, Mineral exploration.

Resumo: Neste trabalho é discutida a correlação estratigráfica de duas estruturas antiforma marcantes da Faixa Piritosa Ibérica (FPI). Por um lado, a região mineira de Neves-Corvo (NC), a maior mina de sulfuretos maciços vulcanogénicos da Europa, intensamente estudada e, por outro, o setor ocidental da estrutura Pomarão-Puebla de Guzmán-Tharsis, uma das mais importantes e completas secções geológicas cartografadas na província. A sequência estratigráfica completa da FPI está representada nos dois setores, nomeadamente, o Grupo Filito-Quartzítico (PQ), seguindo-se o Complexo Vulcano-Sedimentar (CVS) e o Grupo do Flysch do Baixo Alentejo. À escala local, existe maior variabilidade em termos de fácies litológicas, características petrográficas e de idade. O PQ apresenta base de idade desconhecida, sendo compreendido entre o Givetiano médio (Biozona TA) e o Famenniano superior (Biozona LN, Estruniano). O topo é marcado pela presença de níveis de calcários nos dois locais, com idades aproximadas. No CVS observa-se maior variabilidade de idades, nomeadamente ca. 356-330 Ma no Pomarão e ca. 365-346 Ma para toda a área de NC. Na sua base, predominam essencialmente as fácies de xistos negros (Biozonas de Esporos VH a LN), rochas vulcânicas félsicas interdigitadas e sulfuretos maciços, no caso de NC. A sequência sobrejacente do CVS, inclui unidades de xistos siliciosos com nódulos de diferente composição (Biozona de Esporos NM, Viseano médio) e rochas vulcânicas e vulcanogénicas com um espectro de idades com alguma heterogeneidade. Entre este setor e a secção superior do Complexo existe um nível guia, à escala da província, representado por Xistos Borra de Vinho, também presente nas duas áreas de estudo. Acima deste nível ocorrem sedimentos vulcanogénicos e siliciosos de idade Viseano sup. (Biozona de Esporos NM assinalada em NC) e ca. 330 Ma (em níveis vulcânicos no Pomarão). No topo da sequência, há uma transição das unidades do CVS para os turbiditos da Fm. de Mértola (Viseano sup., Biozona de Esporos NM). Salienta-se o facto das idades da base desta formação flysch serem em NC um pouco mais antigas que o topo do CVS no Pomarão. Deste estudo, enfatiza-se uma maior homogeneidade ao nível das formações sedimentares entre as sequências das duas regiões, comparativamente com as intercalações de origem vulcânica, com carácter mais local e maior variabilidade de fácies. A correlação entre as duas estruturas permite identificar cenários favoráveis à prospeção mineral.

Palavras-chave: Neves-Corvo, Pomarão, estratigrafia, geocronologia, prospeção, Faixa Piritosa Ibérica.

[1] Laboratório Nacional de Energia e Geologia (LNEG), Bairro da Vale d´Oca Ap. 14, 7601-909 Aljustrel, Portugal.
[2] Laboratório Nacional de Energia e Geologia (LNEG), Rua da Amieira, 4465-965 S. Mamede de Infesta, Portugal.
[3] Laboratório Nacional de Energia e Geologia (LNEG), Estrada da Portela, Zambujal, Ap. 7586, 2611-901 Amadora, Portugal.
[4] Somincor/Lundin Mining, Stª Bárbara de Padrões, 7780-409 Castro Verde, Portugal.
*Autor correspondente/Corresponding author: luis.albardeiro@lneg.pt

1. Introduction

The Iberian Pyrite Belt (IPB) geology is well known from countless detail mapping campaigns, research projects and mineral exploration programs undertaken by the Portuguese and Spanish geological surveys (LNEG, IGME and Junta de Andalusia), research institutions and private companies since the beginning of last century. On that basis, and addressing similar advancements to the Spanish sector of IPB, it is one of the most important metalogenic provinces in the world for polymetallic VMS deposits. Despite the tremendous volume of geological information, regarding exploration drilling, geophysical data acquisition, geochemical sampling programs and many other data supporting technical and scientific knowledge, several important questions remain unsolved.

Regarding the stratigraphy of IPB, it is almost ubiquos across the entire province to identify the same general rock sequences. Nevertheless, at local scale, the geological sequences based on petrography and traditional stratigraphy cannot always accomplish the paleogeography correlations across the basin.

Concerning the IPB at a regional scale, from Alcácer do Sal in Portugal, to Seville in Spain, one can have in mind an unexpected geological continuity of only two main geological formations, a basement unit with phyllites and quartzites

followed by a suite of mixed volcanic rocks and different types of sediments where VMS-type mineralization is found. When comparing different deposits or different structures and areas within the belt, correlation may not be strait forward, due to lateral and vertical facies variations within the basin, different volcanic centres and also, due to the influence of sync and post tectonic structures.

In this paper, an attempt of geological correlation is made between two key areas of the IPB (Fig. 1): Neves-Corvo mine region, located in the SE sector of the Rosário-Neves-Corvo antiform (Oliveira *et al*., 2013b) and Pomarão, in the westernmost area of the Pomarão-Puebla de Guzmán-Tharsis (PPGT) structure. To attain this goal, previous high-resolution stratigraphy data is used, including U-Pb isotopic age dating in zircons from the felsic volcanic rocks and palynomorph based ages gathered from hosted sedimentary rocks. Previous tectonostratigraphic correlations among the same two areas have been made suggesting that both regions were in the same NW-SE oriented half graben structure (Oliveira *et al*., 2004, 2005, 2006). The correlation between the two structures is important and favourable to the definition of critical exploration scenarios in the IPB central sector.

2. Geological setting of the Iberian Pyrite Belt

The IPB province is a 250 km long and average 50 km wide belthosting the largest concentration of volcanogenic hosted massive sulphide deposits worldwide. Approximately 90 massive sulphide deposits are presently recognized in IPB (10 in Portugal, 80 in Spain), some > 200 Mt (Neves-Corvo, Aljustrel and Rio Tinto) and several others > 100 Mt (Tharsis, Aznalcollar-Los Frailes, Sotiel-Migollas and La Zarza) (Barriga *et al*., 1997; Leistel *et al*., 1998; Sáez *et al*., 1999; Tornos, 2006; Relvas *et al*., 2002, 2006; Jorge *et al*., 2006).

The IPB (Fig. 1) is a NW-SE oriented province included in the "exotic" South Portuguese Zone (SPZ) (Oliveira *et al*., 2006, 2013b, 2019; Inverno *et al*., 2015), the most external and southwesternmost sector of Variscan Orogeny, represented mainly by sedimentary and volcanic rocks of Devonian and Carboniferous age. Structurally, the IPB is interpreted as a thin-skinned, folded and thrusted belt propagating southwards over a mid-crustal basal detachment resulting from the oblique collision of SPZ with Ossa-Morena Zone (OMZ) (Silva *et al*., 1990; Mitjavila *et al*., 1997; Martin-Izard *et al*., 2016).

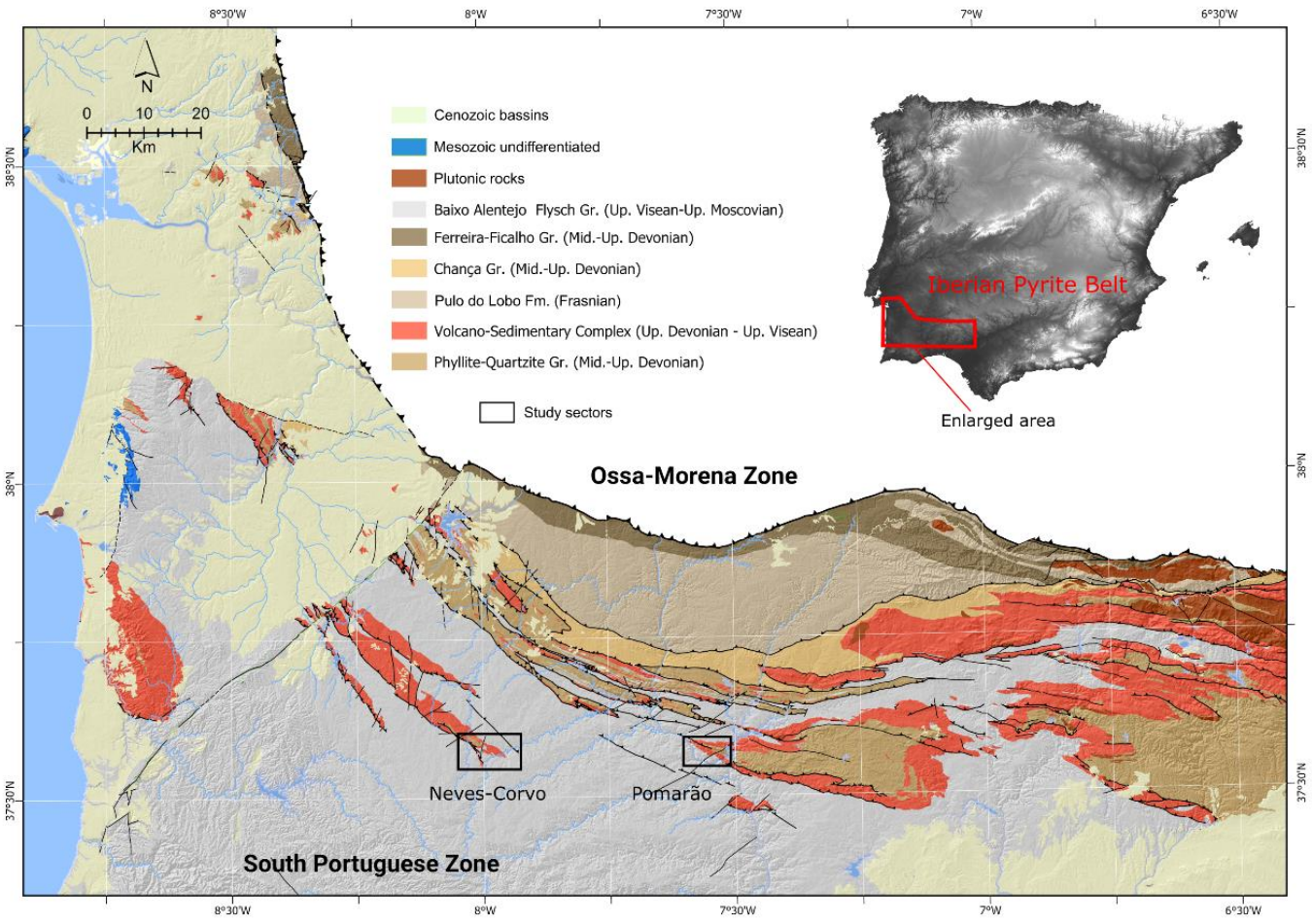

Figure 1. Geological setting of Iberian Pyrite Belt and detail on Neves-Corvo and Pomarão studied areas, located respectively in the SE sector of the Rosário-Neves-Corvo antiform and western sector of the Pomarão-Puebla de Guzmán-Tharsis structure (adapted from Oliveira 1990; Barriga *et al.*, 1997; Leistel *et al.*, 1998; Oliveira *et al*., 2006; Pereira *et al*., 2008; Matos *et al.*, 2008).

Figura 1. Enquadramento geológico da Faixa piritosa Ibérica e detalhe da localização das zonas estudadas, Neves-Corvo e Pomarão, respetivamente no setor SE do antiforma de Rosário – Neves-Corvo e no setor ocidental da estrutura Pomarão – Puebla de Guzmán – Tharsis (adaptado de Oliveira 1990; Barriga *et al.*, 1997; Leistel *et al*., 1998; Oliveira *et al*., 2006; Pereira *et al*., 2008; Matos *et al.*, 2008).

The most recent tectonostratigraphic framework of the IPB (Oliveira *et al*., 2019 and references there in) defines: 1) a southern branch (autochthonous to parautochtonous) which includes pre-orogenic sequences and a syn-orogenic sequence, an intermediate branch with a pre-orogenic sequence and, 2) a northern branch (allochtonous) with a pre-orogenic sequence, a syn-orogenic sequence and an overthrusted pre-orogenic sequence (Oliveira, 1990). In this study we focus on the southern branch sequences where Rosário – Neves-Corvo antiform and Pomarão anticline are located.

The general stratigraphy of IPB (Strauss *et al*., 1977; IGME, 1982; Oliveira, 1990; Leistel *et al*., 1998; Carvalho *et al*., 1999; Tornos, 2006; Oliveira *et al*., 2006; Pereira *et al*., 2007, 2008; Inverno *et al*., 2015; Oliveira *et al*., 2019 and references therein) includes, from base to top: i) the Phyllite-Quartzite Group (PQG); and ii) the Volcano-Sedimentary Complex (VSC), subdivided in some areas (NC and Lousal) in Lower VSC and Upper VSC (Oliveira *et al*., 2013a). Overlaying the VSC sequences is the Baixo Alentejo Flysch Group (BAFG).

The Phyllite-Quartzite Group (PQG) represents the known basement of SPZ as an open siliciclastic platform (Oliveira, 1990, 2019) formed, at least, from Givetian to late Famennian times (González *et al*., 2004, 2005; Pereira *et al*., 2008, 2014; Mendes *et al*., 2018, 2020 in press). Both in Portuguese and Spanish IPB, the PQG outcrops in the core of antiform structures (Oliveira *et al*., 2006), covering larger areas in the Spanish sector. Within the platform deposition environments, the PQG includes dark shales and siliceous lenses (Barranção member in Neves-Corvo), the Phyllite-Quartzite Formation (PQ) and, on top of the sequence, a limestone rich unit named Monte Forno da Cal (in Neves-Corvo area) or Nascedios (in Pomarão anticline) (Oliveira *et al*., 2007, 2019). The PQ is characterized by dark shales with interbedded thin-bedded siltstones and fine grained quartzites which becomes thicker to the top of the sequence, with meter to decametric quartzite and quartzwacke beds (Oliveira *et al*., 2019). Sedimentary structures as cross and massive stratification, ripple current features, bioturbation and parallel lamination are common (Oliveira *et al*., 2006). Despite the PQ Formation base remains unknown, the oldest age recorded indicates AD Miospore Biozone, subzone Lem equivalent to early Givetian age defined in Portugal at the São Francisco da Serra, Caveira and Lousal antiforms (NW IPB region) and at Neves-Corvo mine (Pereira *et al*., 2008, 2010; Matos *et al*., 2014). The uppermost records identify LN Strunian Miospore Biozone of latest Famennian age (Pereira *et al*., 2014, 2020 in press; Mendes *et al*., 2020 in press and references therein). The limestone unit, commonly occurring as discontinuous lenses and nodular shapes, is found on the top of the sequence, frequently with shale intercalations. Fossil record is common, with crinoids and conodont faunas of early-mid Famennian (Boogaard and Schermerhorn, 1981 and references therein). Miospore Biozone LL was identified in the Nascedios limestones (Pereira *et al*., 2008). U-Pb ages in zircons from PQ metasandstones in Spain gave a ca. 366-375 age peak (Pérez-Cáceres *et al*., 2017) meaning the sedimentation process is ca. 366 (mid-Famennian) or younger. In NC, PQ Fm. quartzites were dated with a maximum deposition age of 419 ± 5.5 Ma (Silurian/Devonian boundary, Mendes *et al*., 2018).

The Volcano-Sedimentary Complex (VSC) (Inverno *et al*., 2015; Oliveira *et al*., 2019 and references there in) overlays the PQG rocks and the first volcanic episodes suggest the beginning of the extensional regime in the Upper Devonian basin, since late Famennian to mid-late Visean (Oliveira, 1990; Oliveira *et al*., 2004; Pereira *et al*., 2007, 2014). Lateral facies variations and unit thickness are particularly variable.

The Lower VSC stratigraphy is primary made of black shales comprising felsic and mafic volcanic rocks and massive polymetallic sulphides. Felsic volcanic rocks are dominant (rhyolites, rhyodacites and dacites) over mafic (basalts and dolerites) laying under and/or above the sulphide lenses. Felsic volcanic facies are essentially pumice-rich and coherent facies, related with submarine explosive volcanism and dome and lava flows respectively (Rosa *et al*., 2008, 2016) defining lava-cryptodome-pumice cone volcanos (Rosa *et al*., 2011). The massive sulphide bodies can lay above the felsic volcanic rocks or within the black shales usually with jaspers and carbonates layers closely associated with the mineralization (Leistel *et al*., 1998). Black anoxic shales have been described as favourable lithofacies to host massive sulphides (Sáez *et al*., 2011). The age of these black shales associated with the mineralization is well constrained by palynomorphs assigned to the LN Miospore Biozone of Strunian age (González *et al*., 2002, 2005, 2006; Pereira *et al*., 2008, 2012, 2014; Mendes *et al*., 2017) in several deposits (Neves-Corvo, Lousal, Aznalcollar, and Tharsis), and considered as a key exploration horizon (Pereira *et al*., 2008; 2012; Matos *et al*., 2011). The radiometric age of the volcanic rocks ranges from ca. 374 Ma in the western Cercal area to ca. 339 Ma in Rio Tinto area, defining several volcanic axes subparallel to the SPZ/OMZ boundary. These axes show an evolutionary tendency of the volcanism in space and time from SW to NE within the province (Carvalho, 1976; Barrie *et al*., 2002; Solá *et al*., 2015, 2019; Albardeiro *et al*., in prep).

The Upper VSC (Oliveira *et al*., 2013a, 2019 and references therein), includes a sequence of shales, siliceous shales, Fe-Mn, carbonates and silica-phosphate nodules, siliceous nodules and lenses, ending in one the most widespread marker across the IPB: the radiolarian-rich Purple Shales Formation or *Borra de Vinho*. This is followed by volcanogenic/epiclastic sediments, black shales and fine greywackes defined by essentially dacitic fine grained epiclastic rocks with variable silica/terrigenous component. The presence of fine greywackes on top suggests some gradual transition to the syn-orogenic flysch formations above the VSC.

The Baixo Alentejo Flysch Group (BAFG) follows the VSC expressed as the Mértola Fm. (Mid-Late Visean (Oliveira, 1988, 1990) in almost every IPB areas, with exception of Cercal area where the Mira Fm. (Serpukhovian to middle Bashkirian) is overlaying the VSC. Mértola Fm. includes fine stratified schists, pelites, siltstones and greywackes.

3. Methodology and results

In this work, geochronology data of sediments and volcanic rocks within LNEG's behalf research projects has been used (see legend of figure 6 and table 1 for details). In particular, Geomincor, IPBVectors and EXPLORA LNEG/Lundin Mining joint projects databases and LNEG/IGME/Junta de Andalusia GEO-FPI project data were used. Some of these data has been published (Pereira *et al*., 2014; Solá *et al*., 2015, 2019, Albardeiro *et al*., 2017) or is under preparation (Pereira *et al*., in press). The remaining data will be accessible in this paper. Geological maps here presented have been developed within the GEO-FPI Project based on Portuguese Sheets 7 and 8 (1:200,000) and Andalucia Geological Map (Seville Sheet 1:20,000); 46-C Almodôvar (Oliveira *et al*., 2016) and 46-D Mértola (Oliveira and Silva, 1990) maps (1:50,000) have also been used; Pomarão stratigraphic column is published in 46-D Portugal Geological Map. Stratigraphic column from Neves-

Corvo has been developed within the context of EXPLORA Project.

U-Pb ages in volcanic rocks

In the EXPLORA Project, several exploration drill holes were selected and sampled for palynostratigraphic studies, in sediments, and for U-Pb analysis in zircons from felsic volcanic rocks. For the purpose of this study, five new unpublished samples were selected from EXPLORA goals and considered as representative of the Neves-Corvo mine site geological formations, and studied in this research (Fig. 2, Tab. 1, Appendix). These new results will be compared and complemented with previous and recent published data in both areas. The five samples are derived from four drill holes representing felsic volcanic rocks, classified as rhyolites (Fig. 2, Tab. 1).

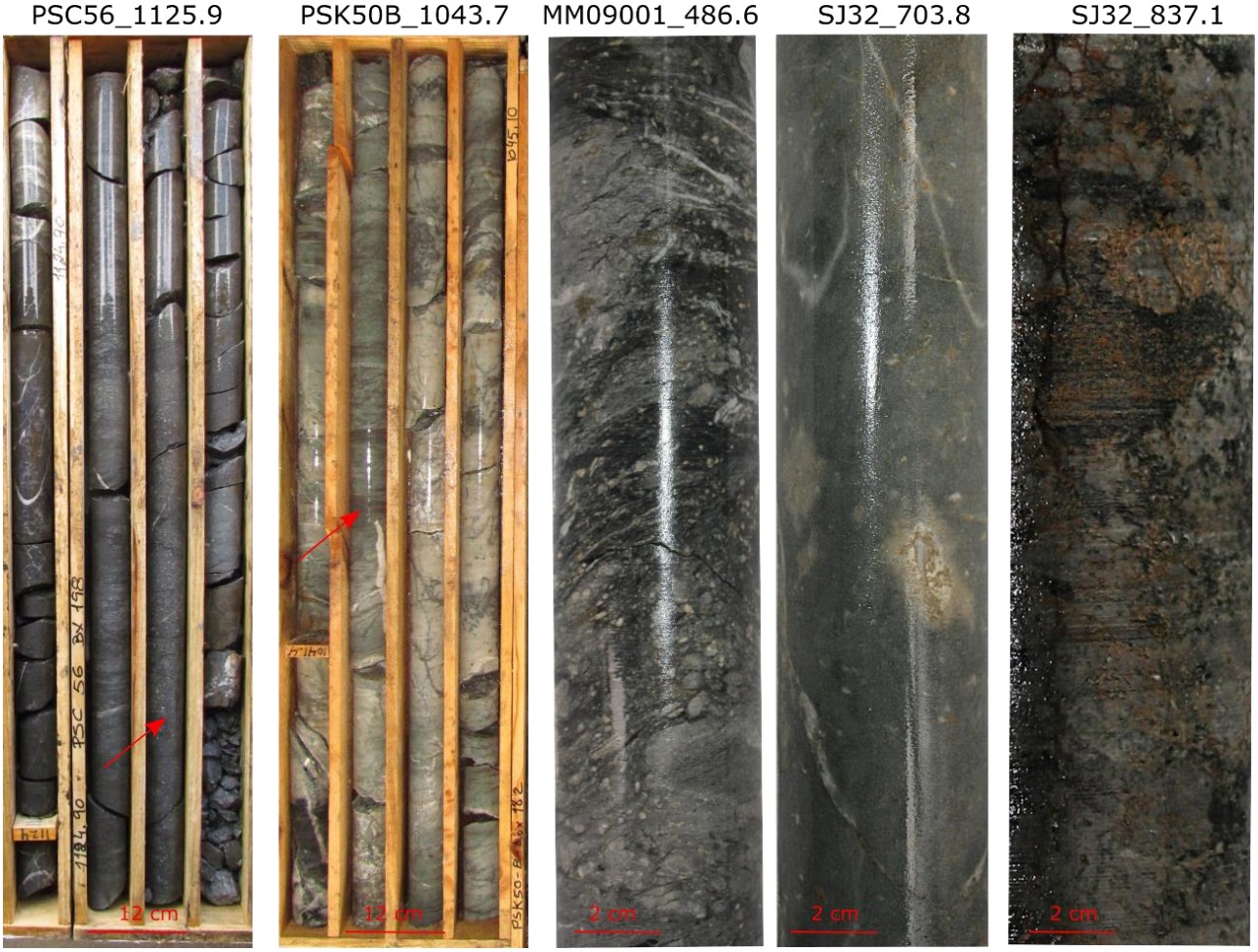

Figure 2. Image of the five rhyolite Neves-Corvo region samples for U-Pb age dating. Samples are designated by drill hole number and depth; PSC56 (1125.9 m), PSK50B (1043.7 m), MM009001 (486.6 m) and SJ32 (703.8 and 837.1 m).

Figura 2. Imagem das cinco amostras de riólitos utilizadas para datação U- Pb. As amostras são designadas pela referência da sondagem e respetiva metragem; PSC56 (1125,9 m), PSK50B (1043,7 m), MM009001 (486,6 m) e SJ32 (703,8 e 837,1 m).

Table 1. U-Pb age results from Neves-Corvo felsic volcanic rocks.

Tabela 1. Resultados das idades U-Pb das rochas vulcânicas félsicas em Neves-Corvo.

Sample*	Area	Formation	Rock-type	Conc. Age (Ma)
SJ32_837.1	Corvo-Semblana	Corvo	Rhyolite	346.8 ± 3.3
SJ32_703.8	Corvo-Semblana	Grandaços (?)	Rhyolite	359.1 ± 3.0** 351.1 ± 3.4/365.0 ± 4.5
PSK50B_1043.7	Semblana	Corvo	Rhyolite	351.3 ± 4.2
MM09001_486.6	Monte Mestres	Grandaços	Rhyolite	366.6 ± 2.0 (see Fig. 2)***
PSC56_1125.9	Rosa Magra	Neves	Rhyolite	345.9 ± 2.8

* Sample number equal to drill core length in the sampled core in meters, EXPLORA/Alentejo2020 Project data. ** One concordia age or two concordia ages. *** See figure 2 for weighted average ages comparison.

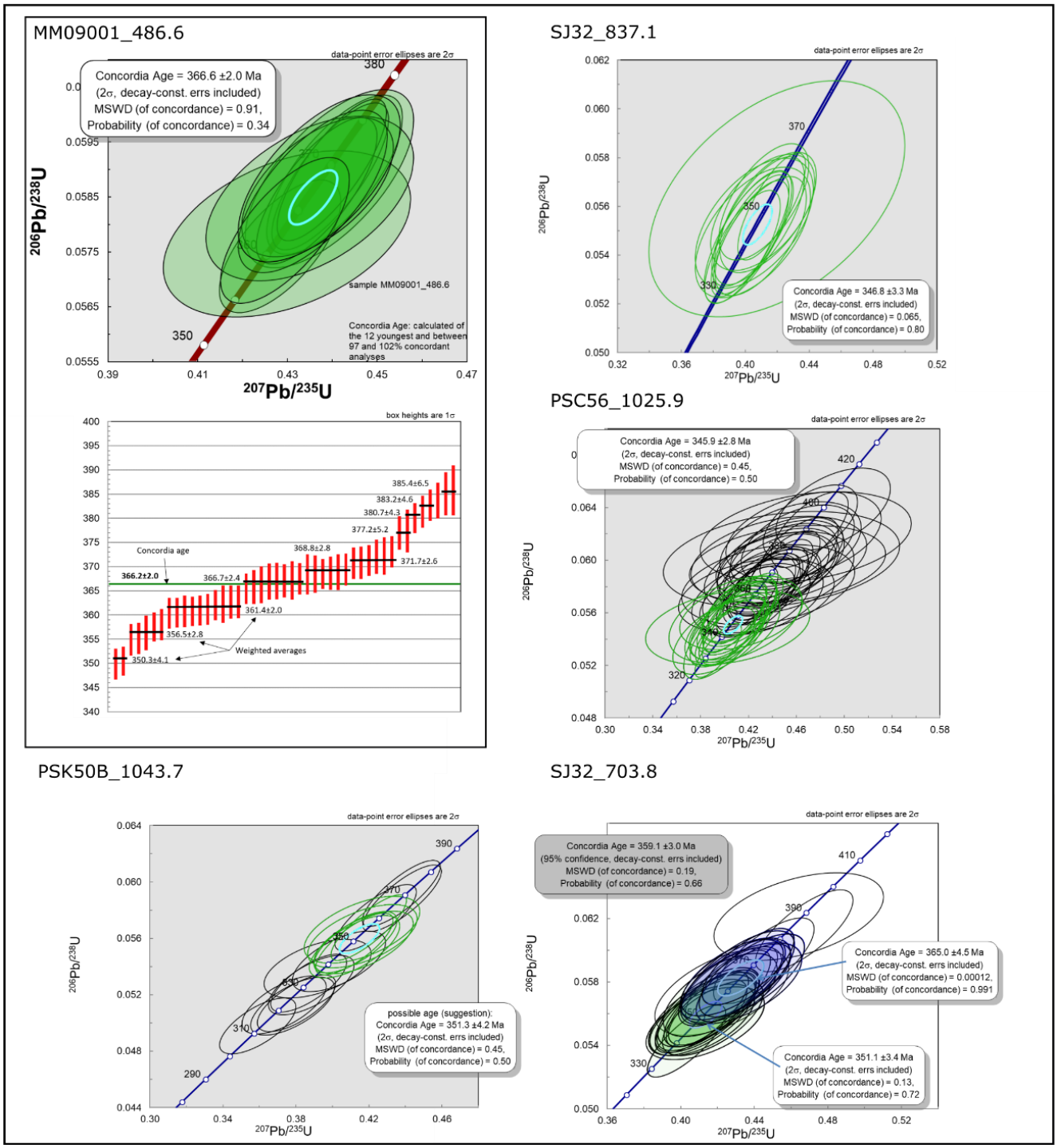

Figure 3. U-Pb concordia ages in zircons from selected volcanic rocks from Neves-Corvo mine site (see Tab. 1 for geological formation setting regarding each sample). Sample SJ32_703.8 shows two possible concordia ages. Sample MM09001_486.6 show significant differences in concordia age and weighted average age interpretation (see text for discussion).

Figura 3. Idades de concordia U-Pb em zircões de rochas vulcânicas selecionadas da área da mina de Neves-Corvo (ver Tab. 1 para enquadramento de cada amostra na respetiva formação geológica). A amostra SJ32_703,8 evidencia duas idades de concordia possíveis. A amostra MM09001_486,6 revela diferenças significativas entre a idade de concordia e a interpretação da idade por médias ponderadas (ver texto para discussão).

Sample MM09001_486.6 represents one of a meter-sized fine to coarse grained porphyritic rhyolite unit identified within the siliceous shales and volcanogenic sediments of the Grandaços Fm. (Upper VSC sequence). SJ32_837.1 is a rhyolite with associated stockwork mineralization interbedded with sediments of the Corvo Fm. (Lower VSC sequence); in the same drill hole, sample SJ32_703.8 represents a coherent facies rhyolite found at the base, or below, the siliceous shales of the Grandaços Fm. and above the Neves Fm.

The stratigraphic position of this rhyolite unit, initially included in the Grandaços Fm., is in discussion once it is affected by footwall and hanging wall faults.

PSC56_1125.9 are felsic volcanic rocks from Neves Fm. and PSK50B_1043.7 sample is from an effusive volcanic and pumice breccia unit from Corvo Fm. (both from Lower VSC sequence).

The samples were submitted to standard procedures for heavy mineral density and magnetic separation (Mange and Maurer, 1992). The obtained zircons (40-180 μm) were epoxy-type resin mounted and coated for back-scattered imaging for target election (Boggs and Krinsley, 2006; Mange and Wright, 2007). Isotopic data acquisition was performed at the Mineralogy and Geology Museum of the Senckenberg Naturhistorische Sammlungen Dresden, Germany, using a Thermo-Scientific Element 2 XR sector field ICP-MS coupled to a New Wave UP-193 Excimer Laser System (*e.g.*, Košler and Sylvester, 2003; Košler, 2007; Guillong, 2004). To enable sequential sampling of heterogeneous grains (*e.g.*, growth zones) during time resolved data acquisition a teardrop-shaped, low volume laser cell was used. Each analysis (laser spot-sizes of 15-35 μm) consisted of 15 s background acquisition followed by 35 s data acquisition. A common-Pb correction based on the interference and background corrected ^{204}Pb signal and a model Pb composition (Stacey and Kramers, 1975) was applied when necessary.

The necessity of the correction is judged on whether the corrected ^{207}Pb/^{206}Pb lies outside of the internal errors of the measured ratios. An Excel® spreadsheet program developed by Axel Gerdes (Institute of Geosciences, Johann Wolfgang Goethe-University Frankfurt) was used for raw data correction for background signal, common Pb, laser induced elemental fractionation, instrumental mass discrimination, and time-dependent elemental fractionation of Pb/Th and Pb/UReported uncertainties were propagated by quadratic addition of the external reproducibility obtained from: (i) the standard zircon GJ-1 (~0.6% and 0.5-1% for the ^{207}Pb/^{206}Pb and ^{206}Pb/^{238}U, respectively) during individual analytical sessions, and (ii) the within-run precision of each analysis. Data interpretation in the form of concordia diagrams was accomplished at 2 sigma error ellipses and concordia ages with 95% confidence interval, using Isoplot 4 (Ludwig, 2009). The ^{207}Pb/^{206}Pb age was taken for data presentation and interpretation for all zircons > 1.0 Ga, and ^{206}Pb/^{238}U ages for younger grains. For further details on the analytical protocol and data processing, see Frei and Gerdes (2009). International Chronostratigraphic chart v2019/07 (www.stratigraphy.org) was followed.

Obtained results are summarized in table 1, concordia ages can be visualized in figure 3 and analytical data in appendix.

4. Neves-Corvo mine region *vs* Pomarão

Anticline geological correlation

The Neves-Corvo structure is known until 1900 m depth with drilling and was studied in more detail using 2D and 3D high-resolution reflection seismics (Carvalho *et al*., 2016; Matos *et al*., 2020). The Pomarão Antiform is less studied with a single SD-P1 393 m drill hole, performed by the Serviço de Fomento Mineiro in the north limb of the structure (Matos and Filipe, 2013) and no seismic data was performed. Besides these constrains, the Neves-Corvo structure shows a complex geometry presenting a PQG parautochthonous main block, but also allochthonous minor blocks observed, for example, in the NE structure of Semblana and Monte Branco sectors (Pereira *et al*., in press). In both cases the fold pattern is conditioned by a significant SW tectonic vergence. At Pomarão Anticline the northern long limb is well exposed showing a Mértola Fm./VSC/PQG normal sequence south of the Salgueiros at the São Domingos mine railway station and main road section (Silva *et al*., 1997; Oliveira and Silva, 2007; Oliveira *et al*., 1998; Oliveira and Matos, 2004). Near the old Pomarão harbour the structure presents a more complex geometry as a common characteristic of the short subvertical limb of the Anticline.

The Phyllite Quartzite Group basement

In Neves-Corvo Antiform and Pomarão Anticline (Figs. 4 and 5), the siliciclastic platform substratum of IPB, represented by the PQG, is found in the anticlinal core structures along a general NW-SE oriented trend. In Neves-Corvo it includes the PQ Formation itself and a limestone-rich lenses unit at the top, the Monte Forno da Cal member, equivalent of Eira do Garcia Member and Nascedios Member limestones, respectively in Pomarão (Figs. 4, 5 and 6).

The PQ Formation in Neves-Corvo, is characterized by dark shales with variable thickness of quartzite beds, ranging from centimetre units, with cross stratification associated with ripple currents features and bioturbation, to decametric/metric, with massive bedding, graded bedding, parallel lamination and syn-sedimentary features, with common lens-shape geometry (Oliveira and Silva, 2007; Oliveira *et al*., 2006). The equivalent Eira do Garcia Member in Pomarão includes dark shales with fine quartzite and silt beds with similar sedimentary features, ripple currents and bioturbation, graded bedding, parallel lamination and others (Boogaard, 1967).

The base of PQ Formation is unknown and the oldest unit ever found in Neves-Corvo corresponds to mid Givetian/mid Frasnian age, TA Miospore Biozones (Mendes *et al*., 2018, 2020 in press). Moreover, a stratigraphic hiatus of ca. 10 Ma from mid Frasnian to late Famennian is recognized (Mendes *et al*., 2018). The Eira do Garcia Member within the PQG of Pomarão Anticline was sampled in SD-P1 drill hole (at 331.4 m) yielding VH Biozone of late Famennian (Fig. 5, Pereira *et al*. 2020) while the youngest age gathered in uppermost PQ Fm. section of Neves-Corvo indicates the LN Biozone of Strunian age (Oliveira *et al*. 2004, 2013a; Pereira *et al*. 2004, 2008, 2014).

In Neves-Corvo, the Monte Forno da Cal limestones are directly overlain by intermediate to mafic volcanic rocks (spilites) (Fig 4). Monte Forno da Cal limestones crops out close to the uppermost section of PQG, corresponding to a decametric layer of dark schists with carbonate lens-shaped beds and nodules (Oliveira *et al*., 2004, 2006). Crinoids are frequently observed. Nascedios Member (Pomarão, Boogaard, 1967) limestones has petrographic correspondence with Monte Forno da Cal limestones, regarding the presence of dark shales and carbonate rich lenses and nodules. Fossiliferous assemblage includes clymenid ammonoids, ortoceras, crinoids, braquiopoda and trilobite remnants, foraminifera, ostracods and conodonts (Oliveira and Silva, 2007; Oliveira *et al*., 2006 and reference therein).

Nascedios Member limestones lenses, in Pomarão antiform, yielded conodonts assigned to the *marginifera* Biozone, a late Famennian age (Boogaard and Schermerhorn, 1981) and palynomorphs assigned to the LL Miospore Biozone of Strunian age (Oliveira and Silva, 2007; Pereira *et al*. 2008). Monte Forno da Cal, in Neves-Corvo, also includes conodonts assigned to the same Famennian *marginifera* Biozone (Boogaard and Schermerhorn, 1981).

Regarding PQG, Neves-Corvo antiform and Pomarão Anticline share the same lithostratigraphy with correlative identical ages (Fig. 6).

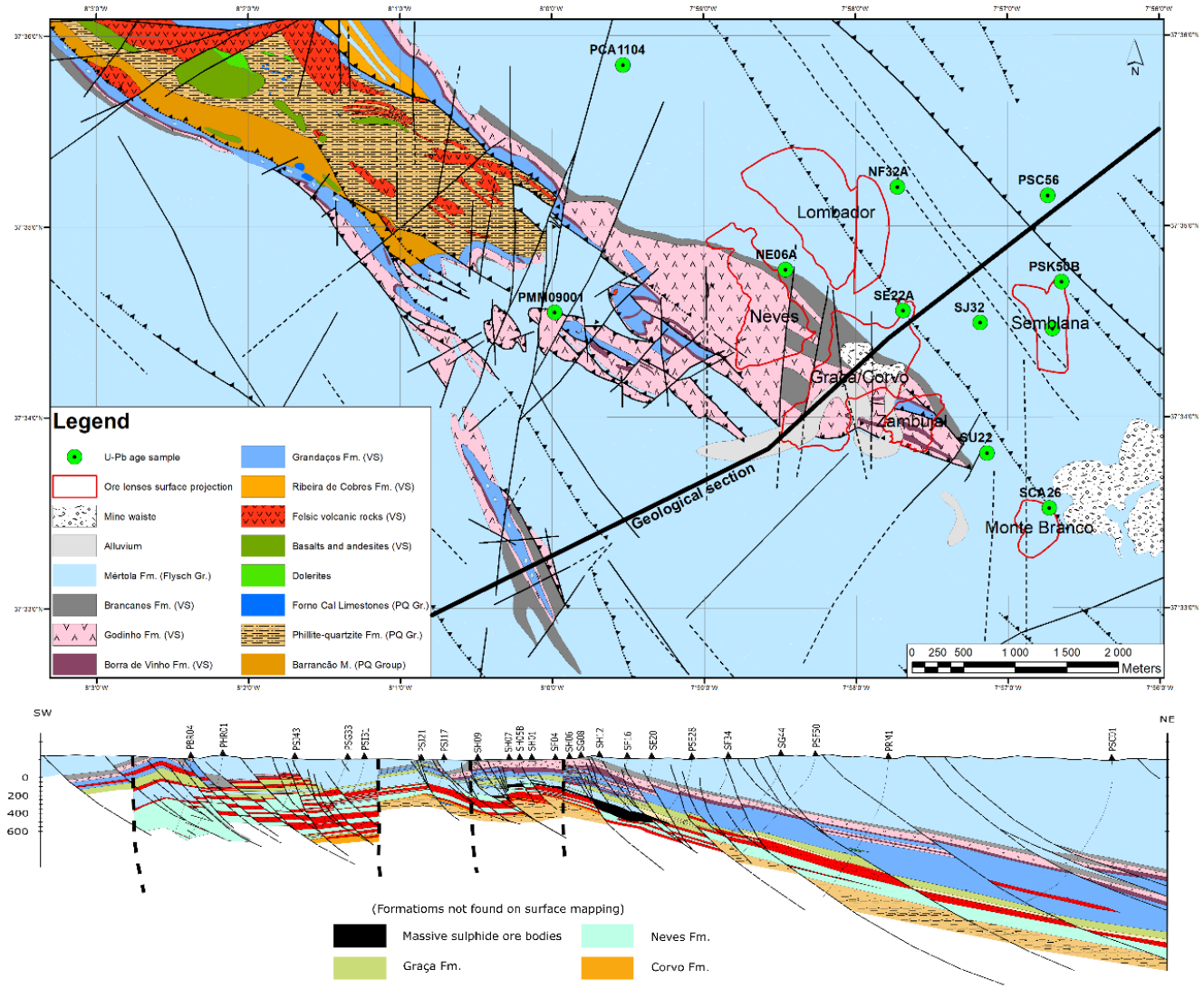

Figure 4. Detail geological mapping and cross-section of Neves-Corvo mine site (adapted from 1:50,000 Portugal Geological Map, Sheet 46-C Mértola, LNEG, Oliveira *et al*., 2016 and Neves-Corvo Region 1:25,000 Geological and Mining Map, LNEG EXPLORA Project).

Figura 4. Cartografia geológica detalhada e secção geológica da região mineira de Neves-Corvo (adaptado da folha 46-C Mértola da Carta Geológica na escala 1:50 000, LNEG, Oliveira *et al*., 2016 e do Mapa Geológico-Mineiro da Região de Neves-Corvo, LNEG Projeto EXPLORA, 1:25 000).

The Volcano Sedimentary Complex

Stratigraphic correlations within the VSC stratigraphy in both studied sectors can be established but some discussion is required (Fig. 6). In Pomarão Anticline, the VSC comprises three formations (Figs. 5 and 6), from bottom upwards: Cerqueirinha Fm., Touril Fm. and Águia Fm. (Boogaard, 1967; Oliveira and Silva, 2007). The second is presently divided in five members (Boogaard, 1967; Oliveira and Silva, 2007): Xistos Negros, Varjotas, Corte Machado, Achada da Mina and *Borra de Vinho* Shales. Regarding Neves-Corvo mine site (Figs. 4 and 6) stratigraphy of the VSC units (Oliveira *et al*., 1997, 2004, 2013a, 2019; Pereira *et al*., 2020 and references therein), a subdivision on Lower VSC and Upper VSC has been considered, with two formations in the former, Neves and Corvo, and five in the second, Graça (and Ribeira de Cobres), Grandaços, Borra de Vinho, Godinho and Brancanes. For description convenience, this subdivision of Lower and Upper VSC is maintained.

Comparing both VSC sequences (Fig. 6), a couple of key correlation horizons can be estimated, as suggested in previous studies (Oliveira *et al*., 2005, 2006). The first corresponds to the black shales unit that carries the mineralization lenses in Neves-Corvo (as well as in Tharsis and Sotiel, Spain, Leistel *et al*., 1998) and appears to be not mineralized in Pomarão area, with equivalent ages. The second horizon is the widespread Borra de Vinho Shales.

Lower Volcano Sedimentary Complex (VSC) sequence

Above the PQG siliciclastic platform the first stages of VSC volcanism have started in late Famennian times. In Neves-Corvo, the Monte Forno da Cal limestones are normally directly overlain by intermediate to mafic volcanic rocks and spilites, also affected by dolerite rocks (Fig 4). In Pomarão, microdiorites and andesites follow the equivalent Nascedios member. An attempt was made to date these last rocks but with no success due to a lack of

zircons. Is Spain, andesite units are also documented and related with the first stages of volcanism and dated close to El Lagunazo mine with Famennian age. Nevertheless, the presence of intermediate to mafic volcanic rocks seems to be coherent from the evolution of the volcanism point of view in both NC and Pomarão.

The Lower VSC units in Neves-Corvo mine region are the Corvo and Neves formations. The former includes dark and black shales, intercalations of carbonate nodules and volcanic clasts (former tuffite, Rosa *et al.*, 2008), formally named "Tufo Brechoide" units (Oliveira *et al.*, 2004), with a late Famennian age (Miospore Biozone VH) (Pereira, 2008). Above and interdigitated with Corvo Fm., the Neves Fm. is characterized by black pyritic shales with thin siltstone beds dated from late Strunian age (Miospore Biozone LN) (Oliveira *et al.*, 2004; Pereira *et al.*, 2008, 2014; Mendes *et al.*, 2017). These biostratigraphy-based ages show contemporaneity with PQG sedimentation. This essentially black shale dominated sedimentary sequence holds several basic and felsic volcanic episodes as well as massive sulphide lenses and jasper/carbonate layers.

Above PQ, mafic volcanic rocks, spilitic lavas, also volcanic sandstones and breccias, directly overlay the PQG limestones as mentioned above, while in others, the felsic volcanic rocks appear not only on top of the siliciclastic platforms units, but even in the PQG sequence.

From this, PQG and VSC contact is not only stratigraphically interdigitated but all paleogeographical transition occurs during LN Miospore Biozone time interval. Corvo Fm. includes rhyolite lavas, hyaloclastites (Munhá *et al.*, 1997), and pumice volcanic breccia (Rosa *et al.*, 2008) yielding an age of 359.3 ± 3.1 Ma (SE22A_773, Solá *et al.*, 2015; Albardeiro *et al.*, 2017) observed in the area of Corvo deposit. Other felsic volcanic rocks interpreted to be within Corvo sediments have been dated ca. 347-351 (SJ32_837.1 and PSK50B_1043.7, this work) on Corvo-Semblana area (Pereira *et al.*, 2020).

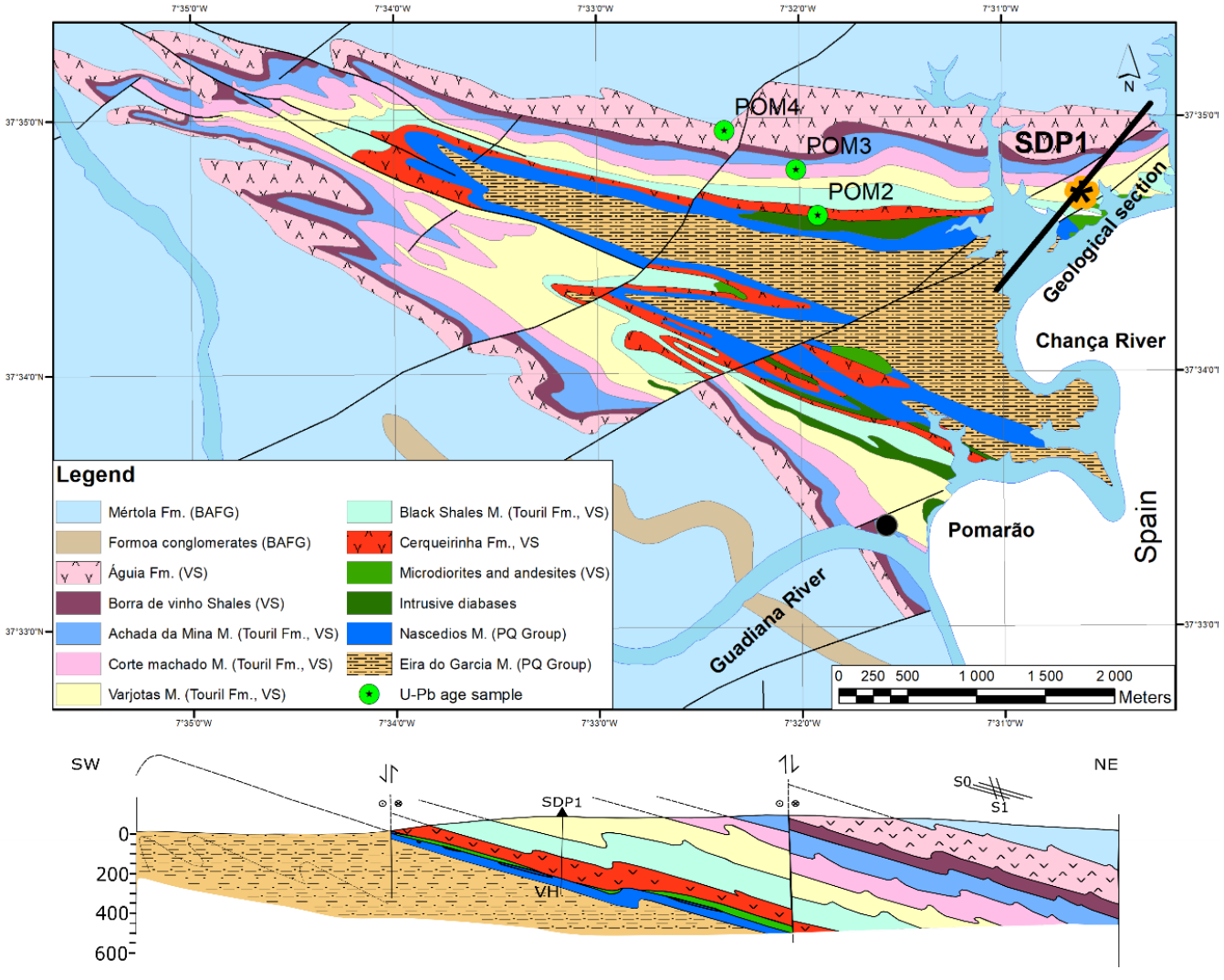

Figure 5. Geological mapping and simplified cross-section of Pomarão anticline structure over SDP1 drill hole (adapted from 1:50,000 Portugal Geological Map, sheet 46-D, SGP/LNEG, Oliveira and Silva, 1990).

Figura 5. Cartografia geológica e secção geológica simplificada da estrutura anticlinal do Pomarão sobre a sondagem SDP1 (adaptada da Folha 46-D Mértola da Carta Geológica de Portugal na escala 1:50,000, SGP/LNEG, Oliveira e Silva, 1990).

Identical rhyolites can be found interfingering within Neves Fm, black shales and unconformable resting on the above Corvo Fm. rocks (Oliveira *et al*., 2004). Most of the Neves-Corvo massive sulphides lenses are found within the Neves Fm. black shales or geometrically above the felsic volcanic rocks. Jaspers and carbonates are found directly above de massive sulphides or near the top of these formations. Dated rhyolites in the mineralization footwall in the Neves ore lens gave a radiometric age of 358.3 ± 3.6 Ma (NE06A_465, Solá *et al*., 2015, Albardeiro *et al*., 2017). Ages ranging from ca. 357-361 Ma in other rhyolite levels within Neves Fm., are found in Neves, Zambujal, Monte Branco footwall lenses and also in the hanging wall sequence of the Lombador deposit. In other areas of Neves-Corvo (Rosa Magra and Semblana, Pereira *et al*., 2020), footwall volcanic rocks within Neves Fm. yield younger ages of ca. 346-352 Ma (see Fig. 6).

The different Neves-Corvo felsic volcanic units/levels mentioned so far within this Lower VSC (Corvo and Neves Fm.) were geochemically studied (Barrett, 2006, 2008), classified according to their volcanic facies (Rosa *et al*., 2008) and compared in terms of radiometric U-Pb age (Albardeiro *et al*., 2017). Three rhyolite types, Rhyolite 1, 2 and 3-types, were identified within this Lower VSC Corvo and Neves formations: i) Rhyolite type-1 is a massive euhedral to sub-euhedral quartz-phyric fiamme rock with quartz and crystal fragments, felsic clasts and disseminated sulphides; ii) Rhyolite type-2 is quartz and feldspar crystal fragments rich, with felsic clasts, mudstone and limestone clasts and rare fiamme (polymitic fiamme sandstone facies); iii) Rhyolite type-3 are coherent rhyolites, quartz and feldspar phyric (10-20% vol.) in a micropoikilitic groundmass, perlitic with quartz-carbonates-chlorite filled amygdales and spherulite and phyllosilicate rich flow bands, jigsaw-fit and clast-rotated monomictic hyaloclastite breccia (Rosa *et al*. 2008). Rhyolite type-1 is richer in Al_2O_3/TiO_2, Zr/TiO_2 and Zr/Al_2O_3 when compared with type 2 and 3, with tholeiitic to calc-alcaline affinity (high Zr/Y). Rhyolites type-2 and 3 show similar Al_2O_3/TiO_2 and Zr/TiO_2 ratios, with lower La/Yb and Zr/Y in type-2 (tholeiitic to calc-alkaline with low Zr/Y) and higher calc-alkaline (high Th/Yb and Zr/Y) to alkaline (low Zr/Nb and high Nb/Y) affinity in type-3. The U-Pb ages of these rhyolites are late Famennian to Tournaisian age (ca. 363-349 Ma) showing a time span of ca. 14 Ma (Solá *et al*., 2015; Albardeiro *et al.*, 2017) in which, two intervals are stated: a late Famennian age rhyolite group (ca. 363-357 Ma) related with mineralization and a Tournaisian age one (ca. 353-349 Ma) representing a late, barren, volcanic episode. From stated studies, the felsic volcanic units found in Lower VSC in Neves-Corvo mine region are different to what chemistry, facies and age is concern, but the presence of two volcanic episodes is proposed (Albardeiro *et al*., 2017).

In Pomarão Anticline, Cerqueirinha Fm. (Boogaard, 1969) rests directly above the PQG rocks, in particular, above the Nascedios unit (limestone lenses and nodules with interdigitations of associated shales). Despite different designations along time, Cerqueirinha Fm. includes felsic volcanic rocks with coherent facies (rhyolites and rhyodacites), hyaloclastites (former felsic tuffs, breccia and agglomerates), peperites and fine volcanogenic rocks (Silva *et al*., 1997; Oliveira *et al*., 1998; Oliveira and Matos, 2004; Oliveira and Silva, 2007). Above this, conformably lies the Xistos Negros Member, the lowermost unit of Touril Fm. (Fig. 6). It is composed of black clayish shales, occasional silty shales, chert lenses and nodules close to the contact with PQG and felsic volcanic lenses with similarities with Cerqueirinha Fm. below (Oliveira and Silva, 2007). U-Pb age dating in Cerqueirinha Fm. felsic volcanic rocks reached 356.8 ± 2.0 Ma (Solá *et al*., 2019) while the Xistos Negros Member age is unknown (although tested for palynostratigraphic studies without positive results). According to mapping and field relations seen in the Pomarão structure northern limb along the old São Domingos mine railway section, an interpreted age of Strunian was given (Oliveira and Silva, 1990; Oliveira *et al*., 1998; Oliveira and Matos, 2004; Oliveira and Silva, 2007).

For this lower part of the VSC sequence, Corvo Fm. (VH Miospore Biozone sediments and ca. 359 Ma and ca. 347-351 Ma rhyolite lavas, hyaloclastites and pumice breccias) and Neves Fm. (LN Mispore Biozone black shales and ca. 346-352 and ca. 357-361 Ma felsic rocks) can be compared with Cerqueirinha Fm. (ca. 357 Ma, in felsic volcanic rocks) and Xistos Negros M. (Late Famennian?). Neves-Corvo mine region ages even suggest two felsic episodes, ca. 346-352 Ma (Tournaisian age) and ca. 357-361 Ma (latest Famennian-early Tournaisian age) (Albardeiro *et al*., 2017), with correspondence of the older one in Pomarão area (ca. 357 Ma). Apparently, the felsic volcanism and the black shale anoxic environment shows more contemporaneity in Neves-Corvo when compared to Pomarão, where a lower volcanic and an upper black shale unit seems to be discernible rather than an interfingering scenario. Oliveira *et al.* (2005) suggests stratigraphic correlation between Neves Fm. (and the associated volcanic rocks) with Cerqueirinha Fm. and Black Shales Member, *i.e*., Corvo Fm. would not have equivalency in Pomarão Anticline stratigraphy. In fact, the above-mentioned ages indicate that older volcanic rocks are approximately contemporaneous in Neves-Corvo and Pomarão. Even considering the common presence of shales and fine volcanic rocks, the associated hyaloclastites and pumice breccia rocks of Corvo Fm. might not be a represented facies in Pomarão. This discussion might also suggest one more volcanic episode in Neves-Corvo mine region than in Pomarão (Oliveira *et al*., 2013b).

Upper Volcano Sedimentary Sequence

If this geological correspondence between Neves-Corvo and Pomarão regions seems obvious considering black shales and felsic volcanic rocks of approximately the same age ranges, further up the sequence the obvious is not the case. In both cases the Upper VSC sequences are well exposed being mapped in detail (Almodôvar and Mértola 1/50,000 maps, Oliveira *et al*., 2016; Oliveira and Silva, 1990). It is particularly the situation of the essentially siliceous shales units found above the black shales productive horizons and below the key horizon Borra de Vinho shales (Fig. 6). This part of the sequence corresponds to a subsection of what has been designated Upper VSC in Neves-Corvo mine region and to some members of the Touril Fm., in Pomarão Anticline. The NC includes Graça and Grandaços formations and the Pomarão embraces Varjotas, Corte Machado and Achada da Mina members (Silva *et al*., 1997; Oliveira *et al*., 1998; Oliveira and Matos, 2004; Oliveira and Silva, 2007). The most important reference here, is the presence of lenses and nodules of different composition in this subsection found in both studied sites.

Graça Fm., in Neves-Corvo region, was not identified on surface mapping, only at depth by drilling. Surface lateral equivalent formation has been suggested, Ribeira de Cobres Fm., mapped further NW from the mine site (Oliveira *et al*., 2013a). The lithology is a monotonous sequence of grey siliceous shales and black shales with a major distinct feature: the presence of centimetre rounded to sub-rounded brownish-black siliceous-phosphatic nodules. Within the shales, some felsic volcanic units and mafic intrusive rocks can be identified.

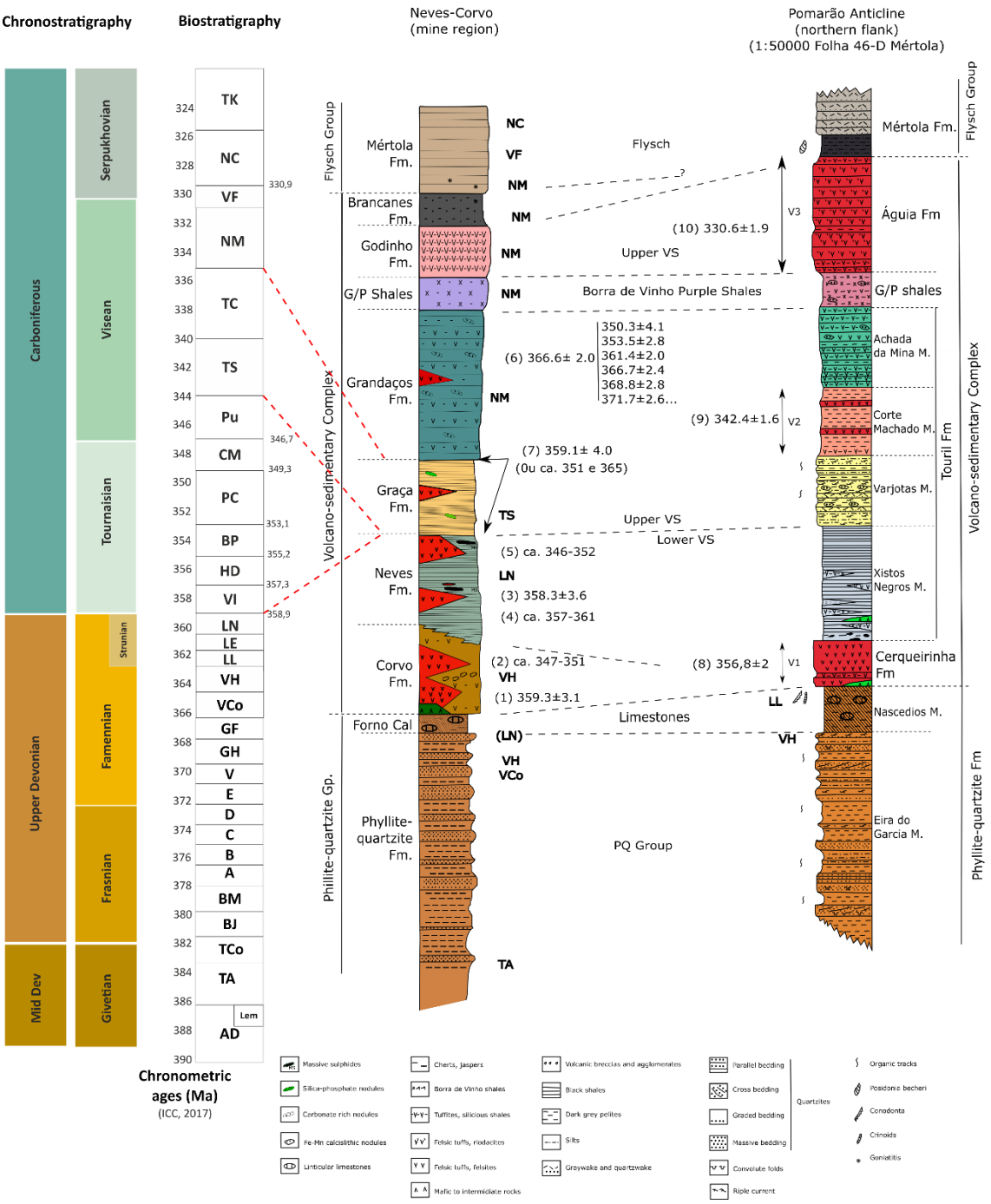

Figure 6. Comparative stratigraphic columns from Neves-Corvo Mine site and Pomarão Anticline with palynological and radiometric ages. (1) Pumice breccia (SE22A_773, Corvo); (2) felsic volcanic rocks (SJ32_837.1 and PSK50B_1043.7, Corvo, Semblana); (3) rhyolite, NE06_455 at mineralization footwall (Neves); (4) felsic volcanic rocks at mineralization footwall SU22_468, CA11041070.2, SCA26_854.65, CA1104_1072.6 (Neves, Zambujal, Monte Branco, Algaré) and hangingwall NF32A_972 (Lombador); (5) same as previous at footwall of upper sulphide lens PSC56_1125.9, PSN44_845.9, PSN44_848.5 (Rosa Magra, Semblana); (6) rhyolite MM09001_486.6 (Monte dos Mestres); (7) felsic volcanic rock SJ32_703.8 (Corvo-Semblana); (8) volcanic breccia POM2 (Pomarão); (9) volcanogenic sediments POM3 (Pomarão); (10) felsic volcanic POM4 (Pomarão). Source: Albardeiro *et al.* (2017) – Ca1104_1070.2, CA1104_1072.6; Solá *et al.* (2015), Albardeiro *et al.* (2017) – NE06_465, SE22A_773; Solá *et al.* (2015) – NF32A_972; Solá *et al.* (2015), Albardeiro *et al.* (2017), Pereira *et al.* (in press) – SU22_468, SCA26_854.65, PSN44_848.5; Solá *et al.* (2019) – POM2, POM3, POM4; This work – SJ32_937.1, PSK50B_1043.7, MM09001_486.6; SJ32_703.8, PSC56_1125.9.

Figura 6. Colunas geológicas comparativas da área da mina de Neves-Corvo e do Anticlinal do Pomarão, com idades palinológicas e radiométricas. (1) brecha *Pumice* (SE22A_773, Corvo); (2) rochas vulcânicas félsicas (SJ32_837.1 e PSK50B_1043.7, Corvo, Semblana); (3) riólito, NE06_455 a muro da mineralização (Neves); (4) rochas vulcânicas félsicas a muro da mineralização SU22_468, CA11041070.2, SCA26_854.65, CA1104_1072.6 (Neves, Zambujal, Monte Branco, Algaré) e a teto NF32A_972 (Lombador); (5) igual ao anterior a muro da lente superior de sulfuretos PSC56_1125.9, PSN44_845.9, PSN44_848.5 (Rosa Magra, Semblana); (6) riólito MM09001_486.6 (Monte dos Mestres); (7) rochas vulcânicas félsicas SJ32_703.8 (Corvo-Semblana); (8) brecha vulcânica POM2 (Pomarão); (9) sedimentos vulcanogénicos POM3 (Pomarão); (10) rocha vulcânica félsica POM4 (Pomarão). Fontes: Albardeiro *et al.* (2017) – Ca1104_1070.2, CA1104_1072.6; Solá *et al.* (2015), Albardeiro *et al.* (2017) – NE06_465, SE22A_773; Solá *et al.* (2015) – NF32A_972; Solá *et al.* (2015), Albardeiro *et al.* (2017), Pereira *et al.* (*in press*) – SU22_468, SCA26_854.65, PSN44_848.5; Solá *et al.* (2019) – POM2, POM3, POM4; Este trabalho – SJ32_937.1, PSK50B_1043.7, MM09001_486.6; SJ32_703.8, PSC56_1125.9.

Felsic rocks show rhyolitic composition interfingering or interbedded with the shales, while mafic rocks are represented by altered dolerites (Oliveira *et al*., 2004). Above the Graça Fm., a general petrographic continuity seems to be present with Grandaços Fm., although siliceous shales with siliceous nodules and lenses are the most common rock type. The major distinction is the presence of lenses and nodules of carbonate composition and flake-like structures instead of previous silica-phosphate. Felsic small units and mafic rocks as dolerites are common and volcaniclastic felsic rocks appear widespread throughout the formation. Concerning Pomarão Anticline, and the rocks laying above the Xistos Negros units, the Varjotas Member is built of fine greywacke sandstones and siltstones interbedded with shales. The main characteristic of this formation is the presence of Fe and Mn oxides and carbonates rich lenses and nodules (Silva *et al*., 1997; Oliveira *et al*., 1998; Oliveira and Matos, 2004; Oliveira and Silva, 2007). In apparent conformity, Varjotas Member is overlain by the Corte Machado Member, a shale-based unit with two intercalations of felsic volcanic rocks. In detail, it includes, from base to top, siliceous dark shales, clayish grey shales, quartz and feldspars greenish grey coarse and fine volcanic rocks, grey shales, fine light sandstones and grey shales. Cherty and aphyric layers are common at the base of both felsic volcanic units.

Further up in the sequence, Achada da Mina Member includes siliceous sandstones, siliceous shales and clay shales with the presence of Mn oxides and carbonates lenses and nodules. From this comparison, two aspects must be discussed.

The first concerns the fact that all shale-based members in both sites are lenses and nodule rich. In Neves-Corvo mine region they are silica-phosphate rich and evolve to carbonate rich, while in Pomarão they remain Fe-Mn-carbonates rich at the base and then essentially Mn oxides and carbonates rich further up the sequence.

First studies are being performed in the Neves-Corvo nodules, and preliminary results in Grandaços Fm. nodules, point to Fe and Mn distinct rich zones in a siliceous matrix; SEM-EDS studies have identified monazite and xenotime as well as the presence of Cu, Co and Sn, Cu and Zn and pyrite (Rosado, unpub. rep., Hércules Laboratory Évora Univ., Explora Project).

The second discussion aspect in this sequence regards the felsic volcanism. In fact, Neves-Corvo felsic volcanic and volcaniclastic rocks exhibit rapid vertical and lateral facies changes and interfingering with the shales throughout the VSC formations.

In Pomarão Anticline, Upper VSC felsic volcanism (below Borra de Vinho shales) seems restricted to Corte Machado Member, and mapping shows a more lateral continuity and consistent width of the felsic volcanic unit all over the anticline structure. This may suggest a more distal volcanic environment with lateral homogeneous depositional facies.

Miospore assemblages assigned to the TS Biozone of early Visean age, were identified in Graça Fm. shales and the NM Miospore Biozone of late Visean age was reported to Grandaços Fm. (Oliveira *et al*., 2004; Pereira *et al*., 2008, 2014). Varjotas Member is interpreted as Tournaisian or early Visean in age, while Corte Machado and Achada da Mina members are inferred to lower Visean (Oliveira and Silva, 2007). These units were also studied for palynostratigraphic ages without positive results. Volcanogenic sediments in Pomarão Corte Machado M. reached a U-Pb age in zircons of 342.4 ± 1.6 Ma (POM3 sample, Fig. 6, Solá *et al*., 2019). In Neves-Corvo, a rhyolite unit, located at the bottom of Grandaços Fm. (this study) and above Neves Fm., yielded 359.1 ± 4.0 Ma (SJ32_703.8); also in Grandaços Fm., a rhyolite rock within the formation obtained a result of 366.6 ± 2.0 Ma (MM09001_486, Fig. 6). These apparent contradicted ages need further interpretation. The ca. 366 age for this rhyolite is a concordia age (i.e., the best computed youngest age of the youngest group of ages) and it is apparently unexplained in the Upper VSC context for a rhyolite. If weighted average ages are taken and interpreted, the following ages peaks are gathered (Fig. 3): 350.3 ± 4.1, 356.5 ± 2.8, 361.4 ± 2.0, 366.7 ± 2.4, 368.8 ± 2.8, 371.7 ± 2.6, 377.7 ± 5.2, 380.7 ± 4.3, 383.2 ± 4.6 and 385.4 ± 6.5. In the SJ32 drill hole sample, with ca. 359 Ma concordia age, two sub-concordia ages can be assumed in this sample, with 351.1 ± 1.4 and 365.0 ± 4.5 Ma. From the above stated data, the volcanic lithologies bounded by a lower (black shales of Neves Fm.) and an upper (Borra de Vinho shales) boundary, within the same biozones envelope, show some inconsistency to what radiometric age is concern. Nevertheless, an age ca. 351 can be attributed to the volcanic rocks close to or at the VSC basement (above Neves Fm.) corresponding to the first concordia age and further up the sequence the youngest peak can be taken at ca. 350 Ma as a possible interpreted age Ma (further Grandaços Fm. age samples should be taken to clarify this interpretation). Also important to state, the rhyolite unit where sample SJ32_703.8 was collected shows fractured footwall and hanging wall contacts, meaning this age interpretation must be taken carefully. From these comparisons, radiometric ages in Neves-Corvo seems older, probably ca. 350, than Pomarão, ca. 342 Ma. for approximately equivalent stratigraphic units. This might reflect an evolutionary trend of the volcanism, together with a long-lasting period of volcanic crystallization process (Albardeiro *et al*., 2019) as shown by the age peaks interpreted in the above sample.

An important issue regarding Neves-Corvo mine region is the imbricated folded tectonic style with low angle thrusting affecting all sequences and units (Silva *et al*., 1990; Oliveira *et al*., 2013a). It is particularly important this late nodules-based shale package overthrusting a lower Flysch sequence which is directly above Neves Fm. and/or the massive sulphides. Minor tangential tectonic is recognized in Pomarão Anticline only referred in the PQG sequence and locally in the Upper VSC sequence (Silva *et al*., 1997; Oliveira *et al*., 1998; Oliveira and Matos, 2004).

The *Borra de Vinho* shales, or the purples shales unit, are the most reliable continuous key horizon in IPB. It is found above this late sequence in both studied sites. In Neves-Corvo it is characterized by interfingering purple and green shales with interbedded lenses and nodules of manganese oxides with typical radiolarian white patches (Oliveira *et al*., 2004). Pomarão unit is made of purple shales interdigitated with green siliceous shales with the same nodules and lenses of Fe-Mn composition and radiolarians (Oliveira and Silva, 2007). The age of this unit is attributed to late Visean (Oliveira and Silva, 2007) and, once the base (Grandaços Fm.) and overlying (Godinho Fm.) normal contact formations have been attributed to NM Miospore Biozone, an identical age can be expected (Pereira *et al*., 2008).

From this late marker horizon to the most recent syn-tectonic Flysch Group there are still the sequences equivalent to the so called V3 volcanism, corresponding to Águia Fm., in Pomarão (Boogaard, 1967), and Godinho Fm. and eventually Brancanes Fm., in Neves-Corvo area. Both Águia and Godinho formations contain metric tuffite units interbedded with fine, grey-greenish siliceous shales and occasional chert lenses (Oliveira *et al*., 2004, Oliveira and Silva, 2007). Some of the volcanogenic sandstone layers within Águia Fm. might be assigned to fine volcanic rocks. Upper and lower contacts are transitional. The uppermost VSC unit in Neves-Corvo, the Brancanes Fm., is made of pyritic black shales with thin graded siltstones and fine greywackes (Oliveira

et al., 2004) with a gradual transition character to the upper turbiditic unit.

Palynological ages in Neves-Corvo mine region yielded NM Miospore Biozone (Pereira *et al*., 2008, 2014) of mid-late Visean age to Godinho Fm., and ammonoid-based late Visean age for Brancanes and Águia formations. This Águia fine felsic volcanic rocks have a radiometric age of 330.6 ± 1.9 Ma (Solá *et al*., 2019), showing an age constancy with the sediments dating.

The Baixo Alentejo Flysch Group

Covering the IPB stratigraphy is the Flysch Group of Baixo Alentejo, here expressed as the Mértola Fm. (Oliveira, 1988, 1990) in both studied sites. As mentioned above in Neves-Corvo mine region, Brancanes Fm. is the uppermost formation of the VSC with a transitional character, but nevertheless, and despite the presence of occasional fine greywacke beds, the presence of pyritic black shales and the fact that it is not a true turbiditic sequence, favours to be considered within the VSC, although pre-flysch facies can suggest otherwise. In Pomarão, a lower facies is individualized although included as a member of Mértola Fm., B0 of M0 Member (Oliveira and Silva, 2007), with fine turbidites, pelites and fine greywackes. IPB source-rocks conglomerates are present showing positive or negative grain selection (Oliveira and Silva, 2007) There are similarities regarding the presence of fine greywacke beds on both units, and the ages were interpreted in the same mid-late Visean age (Fig. 6). Mértola Fm. is made of fine stratified shales (pelites) and turbidites (greywackes and siltstones) interbedded with coarser turbidites (greywackes) of mid-late Visean age (Oliveira, 1988, Oliveira and Silva, 2007, Pereira *et al*., 2008). In Neves-Corvo, based on detail stratigraphy with fine palynological studies, this formation is subdivided in three sequences, namely Mértola 1, 2 and 3, or Mt1, Mt2 and Mt3 (Oliveira *et al*., 2004). In the mine region there are Mt1 shales and greywackes assigned to the NM Miospore Biozone age on surface and Mt2 and Mt3 allochthonous sequences dated of VF and NC Miospore biozones respectively (Oliveira *et al*., 2004; Pereira *et al*., 2008, 2014).

Mértola Fm. is equivalent and a contemporaneous sequence is both studied regions. Nevertheless, it is important to underline that the uppermost volcanic rocks of Pomarão are slightly younger (ca. 330 Ma) than the age assigned to NM Miospore Biozone of Mértola Fm. in Neves-Corvo.

6. Conclusions

An assessment of geological correlation is made among two key areas in Iberian Pyrite Belt, the Neves-Corvo mine region and Pomarão antiform. The former is the most important massive sulphide mine in Europe with detail stratigraphic knowledge based on a huge drilling data base. The second represents the most preeminent complete section exposed on surface of IPB stratigraphy. This correlation has been mentioned (Oliveira *et al*., 2004, 2005, 2006) but without radiometric age data provided in this study.

Main issue regarding this exercise are:

- Both sites confirm the regional stratigraphic sequence, the Phyllite-Quartzite Group (PQG) basement followed by the Volcano-Sedimentary Complex and the Baixo Alentejo Flysch Group laying above.
- The PQG lithostratigraphy allows correlation between Eira do Garcia Member (Pomarão) and PQ Fm. (Neves-Corvo). On top of the sequence, Nascedios (Pomarão) and Forno da Cal (Neves-Corvo) shales and limestones are lithology and stratigraphically equivalents, with ages assigned to LL and LN miospore biozones respectively.
- Above the limestones units, the VSC basement is often marked by intermediate to mafic rocks, as it is the case of basalts and spillites in Neves-Corvo and microdiorites and andesites in Pomarão.
- For VSC correlation purposes, the black shales hosting the massive sulphides and the Borra de Vinho Fm. were used as main key correlation sedimentary horizons.
- Lower VSC in Neves-Corvo mine region, provided the following ages: Corvo Fm. (VH Miospore Biozone in sediments, and ca. 359 Ma and ca. 347-351 Ma in rhyolite lavas, hyaloclastites and pumice breccias); and Neves Fm. (LN Miospore Biozone in black shales, and ca. 346-352 and ca. 357-361 Ma in felsic volcanic rocks). They can be compared with the ages obtained in Pomarão structure, Cerqueirinha Fm. (ca. 357 Ma, in felsic volcanic rocks) and Xistos Negros Member (probably of Strunian age, Oliveira and Silva, 2007). The volcanism is approximately contemporaneous in both sites although the presence of shales and volcaniclastic rocks are common. The hyaloclastites and pumice breccia facies of Corvo Fm. might not be represented in Pomarão. From the two volcanic episodes estimated in Neves-Corvo (Albardeiro *et al*., 2017) only the older seems to be discernible in the Pomarão sequence.
- In Upper VSC, the Graça Fm. shales are early to late Visean in age, while Grandaços Fm. is considered from late Visean ages. Varjotas Member is interpreted as being Tournaisian or early Visean in age, while Corte Machado and Achada da Mina members are inferred to early Visean age. Volcanogenic sediments in Pomarão structure in Corte Machado Member reached 342.4 ± 1.6 Ma. Grandaços Fm. rhyolites yield 366.6 ± 2.0 Ma (with an interpreted younger age peak at ca. 350 Ma) and 359.1 ± 4.0 Ma (ca. 351 and ca. 365 Ma. subconcordia ages). Even considering the ca. 350-351 Ma age, from the above stated data, the radiometric ages are not coherent, needing further research. Also, reasons can be related with migration of the volcanism eastwards.
- Purple shales/green siliceous shales unit recognized in both structures, presents the same nodules and lenses of Fe-Mn composition and radiolarians, and is attributed to mid-late Visean age.
- Both Águia and Godinho formations include volcanogenic sandstones and minor rhyolite volcanic rocks and siliceous shales, the former with fine volcanic units. Brancanes Fm. pyritic black shales/siltstones and fine greywackes has a transition character to the upper turbiditic unit. Palynological ages in Neves-Corvo mine region allowed the identification of the NM Miospore Biozone of late Visean age, to Godinho Fm., and ammonoid-based late Visean age for Brancanes Fm. At Pomarão structure, Águia Fm. fine felsic volcanic rocks have a radiometric age of 330.6 ± 1.9 Ma (Solá *et al*., 2019). An age consistency is verified between two dating methods.
- Mértola Fm. flysch unit is dated from late Visean age, in Pomarão, while in Neves-Corvo mine region three sequences are individualized, ranging from NM to NC Miospore Biozones (mid-late Visean). This stratigraphic unit age correspondence is consistent also from petrographic and paleogeographic perspectives.
- The correlation between the Neves-Corvo and Pomarão sequences is conditioned by the existing data. In the first case the database is very completed with hundreds of exploration drill holes, some of which reached more than 1900 m depth. At the Pomarão region a single drill hole is available with 393 m depth. Besides these constrains, the detail geological mapping data and stratigraphic data allowed doing fine

correlation, useful in mineral exploration. The Lower VSC sequence presents the main potential for VMS deposit exploration.

- This work highlights the presence of the key stratigraphic horizons/formations in IPB and, at a local scale, the heterogeneities amongst lateral units. Moreover, the sedimentary sequences appear to have an age controlled and a stratigraphic continuity within the basin; on the other hand, the volcanic rocks shows some age variability that must be interpreted at the volcanic episode/centre scale and resulting of erosional processes to volcanogenic sediments.

Acknowledgements

The authors thanks to LNEGs research projects: i) GEO-FPI/Interreg POCTEP – *Cross-border observatory for the geo-economic valorisation of Iberian Pyrite Belt*, in association with Instituto Geologico y Minero de España e Junta de Andalucia; ii) EXPLORA project - *Definition of new geological, geophysical and geochemical knowledge vectors applied to Neves-Corvo northern region*, Op ALT20-03-0145-FEDER-000025, funded by Alentejo 2020, Portugal 2020 and European Union (ERDF), in association with Somincor-Lundin Mining and Hercules Laboratory of Évora University; IPBVECTORS - *Geologic, stratigraphic and lithogeochemical characterization of the geological units of the Algaré structure, Rosário Antiform and the Semblana massive sulphide mineralisation*, in association with AGC/Somincor (actual Lundin Mining). Also, thanks are due to Prof. Ulf Linnemann and team, Mandy Hoffmann and Andreas Gartner (Geochronology Lab from Dresden Mineralogy Museum, Germany) for the zircon geochronological data support. Thanks to the S. Mamede de Infesta LNEG's facilities for geochronological sample preparation and supervision, Eng. Ana Botelho, Dr. Ezequiel Ferreira, Margarida Valente and for palynology sample preparation, Irene Sousa. The authors also wish to thank Professor José Brandão da Silva and the anonymous reviewer whose suggestions helped to improve the final result of this paper.

References

Albardeiro *et al*., in prep. The evolution of the volcanic activity in Iberian Pyrite Belt throughout space and time. Geochronology of volcanic VMS-hosted rocks, volcanic lineaments and stratigraphic constrains.

Albardeiro, L., Morais, I., Solá, R., Salgueiro, R., Matos, J. X., de Oliveira, D., Pacheco, N., Araújo, V., 2019. Deciphering U-Pb ages in zircon from Volcano-Sedimentary Complex felsic volcanic rocks. Examples from the Neves-Corvo mining District, Iberian Pyrite Belt, Portugal. EGU General Assembly, 7-12 abril, Viena, Áustria. *Geophysical Research Abstracts*, **21**: EGU2019-15330.

Albardeiro, L., Solá, R., Salgueiro, R., Morais, I., Matos, J., Mendes, M., Pereira, Z., Batista, M. J., Inverno, C., Oliveira, D., Rosa, D., Pacheco, N., 2017. Insights into timing of mineralization in the Neves-Corvo VMS deposit (Iberian Pyrite Belt). *Proceedings of the 14th SGA Biennial Meeting – Mineral Deposits to Discover*, 20-23rd August 2017, Québec City, Canada, **3**: 989-992.

Barrett, T., 2006. *Chemostratigraphy, petrography and alteration of volcanic rocks at the Neves Corvo deposit, Portugal*. Unpublished report for EuroZinc Mining Corporation.

Barrett, T., 2008. *Chemostratigraphy and petrography of volcanic rocks at the Neves-Corvo deposit*, Portugal. Unpub. Rep. for Lundin Mining/Somincor.

Barrie, T., Yamelin, Y., Pascula, E., 2002. U-Pb geochronology of VMS mineralization in the IPB. *Mineralium Deposita*, **37**: 684-703.

Barriga, F., Carvalho, D., Ribeiro, A., 1997. Introduction to the Iberian Pyrite Belt. SEG Neves Field Conference. *Guidebook Series*, **27**: 1-20.

Boggs, S., Krinsley, D., 2006. *Application of Cathodoluminescence Imaging to the Study of Sedimentary Rocks*. Cambridge University Press, 165.

Boogaard, M. V., 1967. *Geology of Pomarão Region (Southern Portugal)*. Thesis, Graffisch Centrum Deltro. Rotherdam, 114.

Boogaard, M. V., Schermerhorn, L. J., 1981. Conodont faunas from Portugal and southwest Spain. Part 6 - A Famennian conodont fauna at Monte Forno da Cal (South Portugal). *Scr. Geol*, **63**: 1-16.

Carvalho, D., 1976. Considerações sobre o vulcanismo da região de Cercal-Odemira: suas relações com a faixa piritosa. *Comunicações dos Serviços Geológicos de Portugal*, **LX**: 215-238.

Carvalho, D., Barriga, F., Munhá, J., 1999. Bimodal Siliciclastic systems: The case of the Iberian Pyrite Belt. *In*: Barrie, C. T., Hannington, M. D. (Eds.), Volcanic associated massive sulphide deposits: Processes and examples in modern and ancient settings. *Reviews Economic Geology*, **8**: 375-408.

Frei, D., Gerdes, A., 2009. Precise and accurate in situ U-Pb dating of zircon with high sample throughput by automated LA-SF-ICP-MS, *Chemical Geology*, **261**: 261-270.

González, F., Moreno, C., López, M. J., Dino, R., Antonioli, L., 2004. Palinoestratigrafía del Grupo Pizarroso-cuarcítico del sector más oriental de la Faja Pirítica Ibérica, SO de España. *Revista Española de Micropaleontología*, **36**: 279-304.

González, F., Moreno, C., Reinaldo, S., Clayton, G., 2002. Ore genesis age of the Tharsis Mining District (Iberian Pyrite Belt): a palynological approach. *Journal of the Geological Society*, London, **159**: 229-232.

González, F., Playford, G., Moreno, C., 2005. Upper Devonian biostratigraphy of the Iberian Pyrite Belt, southwest Spain. *Paleontographica*, **273**: 1-51.

Guillong, M., 2004. *Laser Ablation Inductively Coupled Plasma Mass Spectrometry: Laser ablation system developments and investigations on elemental fractionation*. PhD Thesis, Eidgen Äossischen Technischen Hochschule Züurich, 190.

IGME, 1982. Síntesis geológica de la faja pirítica del SO de Espana. *Servicios Publicaciones Ministerio Industria Energia*, Spain., **98**: 105.

Inverno, C., Díez-Montes, A., Rosa, C., García-Crespo, J., Matos, J., García-Lobón, J. L., Carvalho, J., Bellido, F., Castello-Branco, J. M., Ayala, C., Batista, M. J., Rubio, F., Granado, I., Tornos, F., Oliveira, J. T., Rey, C., Araújo, V., Sánchez-García, T., Pereira, Z., Represas, P., Solá, R., Sousa, P., 2015. Introduction and geological setting of the IPB (Ch.9). *In:* Weihed P. (Ed.), *3D, 4D and predictive modeling of the major mineral belts in Europe*. Berlin, Springer, 191-208.

Jorge, R., Fernandes, P., Rodrigues, B., Pereira, Z., Oliveira, J. T., 2013. Geochemistry and provenance of the Carboniferous Baixo Alentejo Flysch Group, South Portuguese Zone. *Sedimentary Geology*, **284-285**: 133-148.

Jorge, R. C. G. S., Relvas, J. M. R. S., Matos, J. X., 2006. Geochemistry of metasediments from the Phyllite-Quartzite Group, Iberian Pyrite Belt: provenance, source-area weathering and geotectonic implications. *Geochimica et Cosmochimica Acta* Abstracts, **70**(18): A298.

Košler, J., 2007. Laser ablation ICP-MS – a new dating tool in Earth Sciences. *Proccedings Geologial Association*, **118**: 19-24.

Košler, J. Sylvester, P. J., 2003. Present Trends and the Future of Zircon in Geochronology: Laser Ablation ICPMS. *Reviews Mineralogy Geochemistry*, **53**(1): 243-275.

Leistel, J., Marcoux, E., Thieblemont, D., Quesada, C., Sanchez, A., Almodovar, G. R., Pascual, E., Sáez, R., 1998. The volcanic-hosted massive sulphide deposits of the Iberian Pyrite Belt. Review and preface to the special issue. *Mineralium Deposita*, **33**: 2-30.

Ludwig, K. R., 2009. *Isoplot v.4 for Excel 2007*. Berkeley Geochronological Centre, Berkeley, California.

Mange, M., Wright, D., 2007. High-resolution heavy mineral analysis (HRMA): a brief summary. *In*: Mange, M., Wright, D., (Eds.), *Developments in Sedimentology*, **58**: 433-436.

Mange, M. A., Maurer, H. F. W., 1992. *Heavy minerals in colour*. Champan and Hall, London, 147.

Martin-Izard, A., Arias, D., Arias, M., Gumiel, P., Sanderson, D. J., Castañon, C., Sanchez, J., 2016. Ore deposit types and tectonic evolution of the Iberian Pyrite Belt: From transtensional basins and magmatism to transpression and inversion tectonics. *Ore Geology Reviews*, **79**: 254-267.

Matos, J. X., Carvalho, J., Represas, P., Batista, M. J., Sousa, P., Ramalho, E. C., Marques, F., Morais, I., Albardeiro, L., Gonçalves, P., 2020. Geophysical surveys in the Portuguese sector of the Iberian

Pyrite Belt: a global overview focused on the massive sulphide exploration and geologic interpretation. *Comunicações Geológicas*, **107**(III): 41-78 + 3 annexes.

Matos, J. X., Filipe, A., Coord. 2013. Carta de Ocorrências Mineiras do Alentejo e Algarve à escala 1:400000, versão digital. Edição LNEG/ATLANTERRA, Lisboa. ISBN: 978-989-675-029-9.

Matos, J. X., Pereira, Z., Rosa, C., Oliveira, J. T., 2014. High resolution stratigraphy of the Phyllite-Quartzite Group in the northwest region of the IPB, Portugal, *Com. Geológicas*, LNEG, **101**: 489-493. ISSN: 0873-948X.

Mendes, M., Pereira, Z., Matos, J. X., Morais, I., Albardeiro, L., Solá, R., Pacheco, N., Araújo, V., 2018. New preliminary data from Phyllite-Quartzite Formation age based on palynomorphs from Middle-Upper Devonian in Neves-Corvo mine region, Iberian Pyrite Belt (Portugal). *X Congresso Nacional de Geologia*, Vulcânica, **II:** 191-192.

Mendes, M., Pereira, Z., Matos, J. X., Albardeiro, L., Morais, I., Solá, R., Salgueiro, R., Pacheco, N., Araújo, V., Inverno, C., Oliveira, J. T. (2020). New insights on the middle Givetian/middle Frasnian palynofloras from the Phyllite-Quartzite Formation in the Neves-Corvo mine region (Iberian Pyrite Belt, Portugal). *Revue de Micropaléontologie*, **68**: 1-13. http://doi.org/10.1016/j.revmic.2020.100447.

Mendes, M., Pereira, Z., Morais, I., Albardeiro, L., Matos, J. X., 2017. A idade Estruniano (Famenniano superior) da Formação de Neves com base em palinomorfos, mina de Neves-Corvo, Faixa Piritosa Ibérica, Portugal. *A Glimpse of the past. XV. Enc. Jov. Inves. Paleontologia*, Pombal, 279-283.

Mitjavila, J., Martí, J., Soriano, C., 1997. Magmatic evolution and tectonic setting of the Iberian Pyrite Belt volcanism. *Journal Petrology*, **38**: 727-755.

Munhá J, Pacheco, N., Beliz, A., Relvas, J. M. R. S., Hodder, R. W., 1997. Physical and Geochemical Characteristics of the Neves Corvo Felsic Volcanism. *In*: Barriga, F. J. A. S. (Ed.), *Abstracts with Program SEG Neves Corvo Field Conference 1997*, 89.

Oliveira, J. T., 1983. The marine Carboniferous of South Portugal: a stratigraphic and sedimentological approach. *In*: Lemos de Sousa, M. J., Oliveira, J. T. (Eds.), *The Carboniferous of South Portugal*, **29**: 3-38.

Oliveira, J. T., 1990. Stratigraphy and synsedimentary tectonism. *In:* Dallmeyer, R. D., Martinez-Garcia, E., (Eds.), *Pre-Mesozoic Geology of Iberia*. Springer Verlag, 334-347.

Oliveira, J. T. (Coordenador), 1988. Folha 8 da Carta Geológica de Portugal, escala 1/ 200 000, SGP, Lisboa.

Oliveira, J. T., Carvalho, P., Pereira, Z., Pacheco, N., Fernandes, J. P., Korn, D., 1997. The stratigraphy of the Neves Corvo Mine Region. *SEG Guide Book Series*, **27**: 86-87.

Oliveira, J. T., Pereira, Z., Carvalho, P., Pacheco, N., Korn, D., 2004. Stratigraphy of the tectonically imbricated lithological succession of the Neves-Corvo Mine region, Iberian Pyrite Belt. Implications for the regional basin dynamics. *Mineralium Deposita*, **39**: 422-436.

Oliveira, J. T., Pereira, Z., Rosa, C., Rosa, D., Matos, J., 2005. Recent advances in the study of the stratigraphy and the magmatism of the Iberian Pyrite Belt, Portugal. *Journal of Virtual Explorer*, **19**, Paper 9, electronic edition.

Oliveira, J. T., Quesada, C., Pereira, P., Matos, J. X., Solá, A. R., Rosa, D., Albardeiro, L., Díez-Montes, A., Morais, I., Inverno, C., Rosa, C., Relvas, J., 2019. South Portuguese Terrane: A Continental Affinity Exotic Unit, *In*: Quesada, C., Oliveira, T. (Eds.), *The Geology of Iberia: A Geodynamic Approach*, Volume 2: The Variscan Cycle, Regional Geology Reviews, Springer, 173-206.

Oliveira, J. T., Relvas, J., Pereira, Z., Matos, J., Rosa, C., Rosa; D., Munhá, J. M, Jorge, R., Pinto, A., 2006. O Complexo Vulcano-Sedimentar da Faixa Piritosa: estratigrafia, vulcanismo, mineralizações associadas e evolução tectono-estratigráfica no contexto da Zona Sul Portuguesa. *In:* Dias, R., Araújo, A., Terrinha, P., Kullberg, J. C. (Eds.), *Geologia de Portugal no contexto da Ibéria*. Univ. Évora, Évora, 207-243.

Oliveira, J. T., Relvas, J., Pereira, Z., Matos, J., Rosa, C., Rosa, D., Munhá, J., Fernandes, P., Jorge, R., Pinto, A., 2013b. Geologia da Zona Sul Portuguesa, com ênfase na estratigrafia e na vulcanologia física, geoquímica e mineralizações da Faixa Piritosa. *In*: Dias, R., Araújo, A., Terrinha, P., Kullberg, J. C. (Eds.) *Geologia de Portugal Vol. I - Geologia Pré-mesozóica de Portugal*, 673-767.

Oliveira, J. T., Rosa, C., Rosa, D., Pereira, Z., Matos, J. X., Inverno, C. Andersen, T., 2013a. Geology of the Neves-Corvo antiform, Iberian Pyrite Belt, Portugal: New insights from physical volcanology, palynostratigraphy and isotope geochronology studies. *Mineralium Deposita*, **48**: 749-766.

Oliveira, J. T., Silva, J., 1990. *Folha 46-D Mértola da Carta Geológica de Portugal à escala 1:50 000*. Serviços Geológicos de Portugal.

Oliveira, J. T., Silva, J., 2007. *Noticia Explicativa da Folha 46-D, Mértola da Carta Geológica de Portugal na escala 1:50 000*. Dep. Geologia. INETI, 1-46.

Pereira, Z., Matos, J. X., Solá, R., Batista, M. J., Salgueiro, R., Rosa, C., Albardeiro, L., Mendes, M., Morais, I., de Oliveira, D., Pacheco, N., Araújo, V., Castelo Branco, J. M., Neto, R., Lains Amaral, J., Inverno, C., Oliveira, J. T. 2020, in press. Geology of the recently discovered massive and stockwork sulphide mineralisation of Semblana, Rosa Magra and Monte Branco, Neves-Corvo mine region, Pyrite Belt, Portugal, Geological Magazine.

Pereira, Z., Fernandes, P., Matos J. X., Jorge, R., Oliveira, T., 2018. Stratigraphy of the Northern Pulo do Lobo Domain, SW Iberia Variscides: A palynological contribution. *Geobios*, **51**(6): 491-506.

Pereira, Z., Fernandes, P., Matos J. X., Jorge, R., Oliveira, J. T., 2019. Reply to 'Comment on "Stratigraphy of the Northern Pulo do Lobo Domain, SW Iberia Variscides: A palynological contribution". *Geobios*, **51**(6): 491-506.

Pereira, Z., Fernandes, P., Oliveira, J. T., 2006. The Upper Devonian Palynostratigraphy and Organic Matter Maturation of the Pulo do Lobo Domain, South Portuguese Zone, Portugal. *Comunicações Geológicas*, **93**: 23-38.

Pereira, Z., Matos, J., Fernandes, P., Jorge, R., Oliveira, J. T., 2010. Qual a idade mais antiga da Faixa Piritosa? Nova idade Givetiano inferior para o Grupo Filito-Quartzítico (Anticlinal de S. Francisco da Serra, Faixa Piritosa). VIII Congresso Nacional de Geologia, *E-Terra*, **17**(3): 1-4.

Pereira, Z., Matos, J., Fernandes, P., Oliveira, J. T., 2007. Devonian and Carboniferous palynotratigraphy of the South Portuguese Zone, Portugal – An overview. *Comunicações Geológicas*, **94**: 53-79.

Pereira, Z., Matos, J. X., Batista, M. J., Solá, R., Salgueiro, R., Oliveira, D., Oliveira, J. T., Inverno, C., Rosa, C., 2014. Caracterização geológica, estratigráfica e litogeoquímica das unidades geológicas da zona do Algaré, Antiforma do Rosário e da mineralização de sulfuretos maciços da Semblana. Rel. Proj. IPB Vectors, LNEG/Lundin Mining, 150.

Pereira, Z., Matos, J. X., Fernandes, P., Oliveira, J. T., 2008. Palynostratigraphy and Systematic Palynology of the Devonian and Carboniferous Successions of the South Portuguese Zone, Portugal. *Memorias INETI*, **34**: 1-176.

Pereira, Z., Matos, J. X., Rosa, C., Oliveira, J. T., 2012. Palynostratigraphic importance of the Strunian in the Iberian Pyrite Belt. *45th Annual Meeting AASP and Cimp*, Lexington, KY, USA, 42-43.

Pereira, Z., Mendes, M., Diez Montes, A., Matos, J. X., 2020. Atividade A1.2. Datações de rochas sedimentares com base em Palinologia. *GEO-FPI: Observatorio Transfronterizo para la Valorización Geo-Económica de la Faja Pirítica Ibérica*. Unpublished report. 129.

Pereira, Z., Pacheco, N., Oliveira, J. T., 2004. A case of applied palynology: dating the lithological succession of the Neves-Corvo mine, Iberian Pyrite Belt, Portugal. *In:* Wong, T (Ed.), *Proceedings of the XVth ICCP Stratigraphy*, R. D. Academy Arts and Sciences, 345-354.

Pérez-Cáceres, I., Martínez Poyatos, D., Simancas, L., Azor, A., 2017. Testing the Avalonian affinity of the South Portuguese Zone and the Neoproterozoic evolution of SW Iberia through detrital zircon populations *Gondwana Research*, **42**: 177-192.

Relvas, J., Barriga, F., Ferreira, A., Noiva, P., Pacheco, N., Barriga, F., 2006. Hydrothermal alteration and mineralization in the Neves-Corvo volcanic hosted massive sulphide deposit, Portugal. I. Geology, mineralogy, and geochemistry. *Economic Geology*, **101**: 753-790.

Relvas, J. M. R. S, Barriga, F. J. A. S, Pinto, A. M. M., Ferreira, A, Pacheco, N, Noiva, P. C., Barriga, G., Baptista, R., Carvalho, D., Oliveira, V., Munhá, J., Hutchinson, R., 2002. The Neves-Corvo deposit, Iberian Pyrite Belt, Portugal - impacts and future, 25 years after the discovery. *Society Economic Geologist Special Publication*, **9**: 155-176.

Rosa, C., McPhie, J., Relvas, J., 2011. Sediment-matrix igneous breccias at the top contacts of felsic units in the IPB: implications for VHMS exploration. *11th SGA Biennial Meeting: Let´s Talk Ore Deposits*. Antofagasta, Chile. s2.6.5: 754-756.

Rosa, C., McPhie, J., Relvas, J., 2016. Distinguishing peperite from other sediment-matrix igneous breccias: Lessons from the Iberian Pyrite Belt. *Journal of Volcanology and Geothermal Research*, **315**: 28-39.

Rosa, C., Mcphie, J., Relvas, J., Pereira, Z., Oliveira, J. T., Pacheco, N., 2008. Volcanic setting of the giant Neves-Corvo massive sulfide deposit, Iberian Pyrite Belt, Portugal. *Mineralium Deposita*, **43**: 449-466.

Rosado, L., 2019. Unpub. Rep for EXPLORA Project.

Sáez, R., Moreno, C. and González, F., 2011. Black shales and massive sulfide deposits: causal or casual relationships? Insights from Rammelsberg, Tharsis, and Draa Sfar. *Mineralium Deposita*, **46**: 585-614.

Sáez, R., Pascual, E., Toscano, M., Almodóvar, G. R., 1999. The Iberian type of volcano-sedimentary massive sulphide deposits. *Miner. Deposita*, **34**: 549-570.

Silva, J. B., 1997. The geodynamic setting of the South Portuguesa Zone from a structural point of view. *In*: Neves Corvo Field Conference: Geology and VMS Oeposits of the lberian Pyrite Belt. Barriga, F., Carvalho, O. (Eds.), Society of Economic Geologists. *Guidebook Series, Field Trip 2*. Maio de 1997. **27**: 114-124.

Silva, J. B., Oliveira, J. T., Ribeiro, A., 1990. South Portuguese Zone.Structural outline. *In:* Dallmeyer, R. D. and Martinez Garcia, E. (Eds.), *Pre-Mesozoic Geology of Iberia*., Springer Verlag, 348-362.

Solá, R., Albardeiro, L., Salgueiro, R., Morais, I., Díez-Montes, A., Matos, J. X., 2019. Idades U-Pb em rochas vulcano-sedimentares da Zona Sul Portuguesa: resultados preliminares do Projeto GEO-FPI. *Livro de Resumos do XII Congresso Ibérico de Geoquímica – XX Semana da Geoquímica*, 87-90.

Solá, R., Salgueiro, R., Pereira, Z., Matos, J. X., Rosa, C., Araújo, V., Neto, R., Lains, J. A., 2015. Time span of the volcanic setting of the Neves Corvo VHMS deposit. *Livro Resumos Cong. Ibérico Geoquímica/XVIII Semana Geoquímica*, 120-123.

Stacey, J. S., Kramers, J. D., 1975. Approximation of terrestrial lead isotope evolution by a two-stage model. *Earth Planet Science Letters*, **26**: 207-221.

Strauss, G. K., Madel, J., Fernández Alonso, F., 1977. Exploration practice for strata-bound volcanogenic sulphide deposits in the Spanish-Portuguese Pyrite Belt: Geology, geophysics, and geochemistry. *In*: Klemm, D. D., Schneider, H. J. (Eds.), *Time and stratabound ore deposits*. Berlin, Springer-Verlag, 55-93.

Tornos, F., 2006. Environment of formation and styles of volcanogenic massive sulfides: The Iberian Pyrite Belt. *Ore Geology Reviews*, **28**: 259-307.

Appendix. U-Pb laser ablation results of the samples presented in this research.
Apêndice. Resultados da ablação laser U-Pb das amostras apresentadas neste estudo.

Sample SJ32_703.8
Amostra SJ32_703.8

Number	^{207}Pb[a] (cps)	U[b] (ppm)	Pb[b] (ppm)	Th[b] U	^{206}Pb ^{204}Pb	^{206}Pb[c] ^{238}U	2 σ %	^{207}Pb[c] ^{235}U	2 σ %	^{207}Pb[c] ^{206}Pb	2 σ %	rho[d]	^{206}Pb ^{238}U	2 σ (Ma)	^{207}Pb ^{235}U	2 σ (Ma)	^{207}Pb ^{206}Pb	2 σ (Ma)	conc %
A-19	4608	222	11	20.75	0.22	0.05238	3.5	0.41480	6.2	0.05745	5.1	0.56	329	11	352	19	508	113	65
A-21	33117	1532	82	0.64	0.09	0.05427	4.0	0.40980	4.7	0.05478	2.4	0.85	341	13	349	14	403	55	85
A-22	7294	327	18	0.15	0.13	0.05593	3.7	0.41160	5.8	0.05339	4.4	0.64	351	13	350	17	345	100	**102**
A-24	26819	1155	65	46.57	b.d.	0.05670	3.5	0.43850	4.2	0.05611	2.4	0.83	356	12	369	13	456	52	78
A-25	11202	441	25	0.17	0.33	0.05741	3.6	0.46900	4.9	0.05926	3.3	0.74	360	13	390	16	576	72	62
A-32	11398	429	25	0.15	0.81	0.05836	3.4	0.46980	6.0	0.05840	4.9	0.57	366	12	391	19	544	108	67
A-33	5159	229	13	0.21	0.11	0.05798	3.9	0.42800	5.6	0.05355	4.0	0.70	363	14	362	17	352	90	**103**
A-34	7202	290	16	0.14	0.21	0.05749	3.5	0.43540	5.7	0.05495	4.5	0.62	360	12	367	18	410	100	88
A-37	12857	514	24	31.09	2.11	0.04684	4.4	0.47590	8.8	0.07371	7.7	0.49	295	13	395	29	1033	156	29
A-38	8963	380	18	0.24	0.71	0.04884	3.4	0.40990	5.7	0.06088	4.6	0.60	307	10	349	17	634	99	48
A-39	6602	293	17	0.12	0.14	0.05829	4.1	0.43110	5.9	0.05365	4.2	0.70	365	15	364	18	356	94	**103**
A-41	8536	355	18	0.95	1.06	0.05237	4.0	0.40490	6.6	0.05610	5.3	0.60	329	13	345	19	456	117	72
A-42	9262	470	23	16.15	0.85	0.05040	3.7	0.38760	5.4	0.05580	4.0	0.67	317	11	333	15	444	90	71
A-43	20901	935	50	58.81	b.d.	0.05469	3.4	0.41810	4.0	0.05546	2.1	0.85	343	11	355	12	430	48	80
A-44	8518	390	22	0.45	0.35	0.05641	3.6	0.41530	5.5	0.05340	4.1	0.66	354	12	353	16	345	93	**102**
A-45	4704	199	11	0.60	0.24	0.05636	3.9	0.44370	7.8	0.05711	6.7	0.51	353	14	373	24	495	147	71
A-47	10722	469	27	0.28	0.11	0.05933	3.7	0.44510	5.0	0.05442	3.4	0.74	372	13	374	16	388	75	**96**
A-48	8487	282	16	0.12	1.73	0.05696	3.6	0.44010	6.4	0.05606	5.3	0.56	357	12	370	20	454	118	79
A-50	17698	718	43	0.16	b.d.	0.06123	3.5	0.46720	4.6	0.05536	3.1	0.75	383	13	389	15	426	69	90
A-56	3745	159	9	60.51	b.d.	0.05427	3.6	0.46560	6.1	0.06224	4.9	0.60	341	12	388	20	682	104	50
A-59	9692	438	25	0.37	1.14	0.05737	3.9	0.42230	7.0	0.05341	5.9	0.55	360	14	358	21	346	133	**104**
A-60	12552	568	31	0.29	0.10	0.05557	3.5	0.43480	4.5	0.05676	2.8	0.78	349	12	367	14	482	62	72
A-61	17626	823	43	63.64	0.12	0.05323	3.4	0.40820	4.8	0.05564	3.4	0.70	334	11	348	14	437	76	76
A-63	8614	389	21	0.23	0.21	0.05611	3.8	0.41150	5.0	0.05321	3.3	0.75	352	13	350	15	337	76	**104**
A-64	8320	367	21	0.12	0.16	0.05796	3.4	0.43420	4.8	0.05435	3.4	0.71	363	12	366	15	385	77	**94**
A-65	7834	336	18	0.10	0.22	0.05574	3.5	0.41750	5.4	0.05433	4.1	0.65	350	12	354	16	384	92	**91**
A-67	10939	534	29	0.57	0.32	0.05540	3.4	0.41340	6.4	0.05413	5.4	0.53	348	11	351	19	376	122	**92**
A-68	6479	288	15	0.21	0.03	0.05399	3.7	0.40490	5.4	0.05441	3.9	0.69	339	12	345	16	387	87	88
A-69	13596	600	27	0.24	0.17	0.04572	4.6	0.33580	5.5	0.05329	3.0	0.83	288	13	294	14	340	69	85
A-70	6433	269	15	0.19	0.30	0.05602	3.4	0.44090	4.5	0.05709	3.0	0.74	351	11	371	14	494	67	71
A-71	7712	316	17	0.16	0.19	0.05623	3.4	0.42440	5.6	0.05476	4.5	0.60	353	12	359	17	402	101	88
A-72	1683	72	4	0.77	0.70	0.06213	3.6	0.46410	8.1	0.05420	7.3	0.45	389	14	387	26	379	163	**103**
A-73	11946	551	28	0.10	0.09	0.05239	3.6	0.39880	4.7	0.05522	3.0	0.77	329	12	341	14	420	67	78
A-74	20759	964	52	56.76	b.d.	0.05448	3.4	0.41320	4.6	0.05502	3.0	0.75	342	11	351	14	412	68	83
A-81	10020	471	23	0.49	0.30	0.04987	3.9	0.38840	5.7	0.05650	4.2	0.68	314	12	333	16	472	93	67
A-82	4000	164	9	0.10	0.19	0.05820	3.6	0.42980	5.7	0.05357	4.4	0.63	365	13	363	17	352	100	**103**
A-83	12013	526	30	0.13	0.23	0.05827	3.4	0.42810	5.3	0.05330	4.1	0.64	365	12	362	16	341	92	**107**
A-84	8211	356	19	0.11	0.27	0.05534	3.4	0.41560	5.8	0.05448	4.7	0.59	347	12	353	17	390	106	89
A-85	5389	290	14	12.64	0.75	0.04806	3.7	0.36050	7.0	0.05442	5.9	0.54	303	11	313	19	388	131	78
A-86	9981	487	24	0.18	0.51	0.04941	3.5	0.36720	5.0	0.05392	3.6	0.70	311	11	318	14	367	82	85
A-87	9531	418	24	0.15	0.14	0.05842	3.7	0.43880	5.3	0.05449	3.9	0.68	366	13	369	17	391	87	**94**
A-88	8590	406	21	0.32	0.12	0.05219	3.6	0.39670	5.2	0.05514	3.7	0.70	328	12	339	15	417	82	79
A-89	7334	340	19	0.19	0.29	0.05593	3.3	0.41160	4.9	0.05339	3.6	0.67	351	11	350	14	345	82	**102**
A-90	8163	375	21	0.15	0.22	0.05632	3.3	0.41730	4.7	0.05375	3.3	0.71	353	11	354	14	360	74	**98**
A-91	12953	462	23	0.23	2.44	0.05133	3.7	0.39280	6.4	0.05552	5.3	0.57	323	12	336	18	433	117	75
A-92	6244	262	14	0.19	0.24	0.05393	3.7	0.43450	5.9	0.05845	4.6	0.63	339	12	366	18	546	101	62
A-93	8968	427	23	0.37	0.14	0.05532	3.5	0.41780	4.8	0.05479	3.4	0.72	347	12	355	14	403	75	86
A-96	9678	340	18	0.22	1.37	0.05434	3.5	0.43040	5.7	0.05746	4.6	0.61	341	12	363	18	509	100	67
A-97	6590	301	17	0.11	0.16	0.05898	3.3	0.43670	4.7	0.05372	3.3	0.71	369	12	368	14	359	74	**103**
A-98	8018	373	21	0.46	0.36	0.05635	3.5	0.41670	5.1	0.05365	3.6	0.69	353	12	354	15	356	82	**99**
A-99	7780	353	19	0.23	0.22	0.05611	3.7	0.41350	5.4	0.05347	4.0	0.68	352	13	351	16	348	90	**101**
A-100	9553	461	25	0.12	0.20	0.05428	3.4	0.40320	4.3	0.05389	2.6	0.79	341	11	344	13	366	60	**93**
A-106	9644	399	21	0.12	0.67	0.05358	3.4	0.42400	4.9	0.05741	3.5	0.70	336	11	359	15	507	77	66
A-108	10432	453	24	0.50	0.15	0.05318	3.4	0.44220	4.4	0.06033	2.8	0.77	334	11	372	14	615	61	54
A-109	8255	438	20	2.81	1.12	0.04539	3.8	0.33200	7.7	0.05307	6.8	0.49	286	11	291	20	331	154	86
A-110	23489	1115	59	53.95	b.d.	0.05413	3.3	0.41430	3.9	0.05553	2.0	0.85	340	11	352	11	433	45	78
A-111	14328	657	37	0.11	0.06	0.05695	4.4	0.42050	5.5	0.05357	3.4	0.79	357	15	356	17	353	76	**101**
A-112	11079	554	29	5.35	1.01	0.05361	3.8	0.44940	5.2	0.06082	3.7	0.72	337	12	377	17	632	79	53
A-113	5390	217	12	0.11	0.66	0.05791	3.6	0.43310	6.2	0.05425	5.0	0.59	363	13	365	19	381	112	**95**
A-114	12113	555	32	0.18	0.11	0.05782	3.4	0.42760	4.8	0.05366	3.3	0.72	362	12	361	15	356	75	**102**
A-116	8353	396	21	0.21	0.22	0.05327	3.3	0.39940	5.2	0.05439	4.0	0.64	335	11	341	15	387	89	87
A-117	5843	267	15	6.68	0.17	0.05785	3.3	0.42770	5.2	0.05363	4.0	0.64	363	12	362	16	355	89	**102**
A-118	32501	1694	93	1.45	0.42	0.05562	3.3	0.41170	5.7	0.05370	4.6	0.58	349	11	350	17	358	104	**98**
A-120	7567	363	20	0.19	0.07	0.05718	3.8	0.42150	6.0	0.05349	4.7	0.62	358	13	357	18	349	106	**103**

Sample SJ32_837.1
Amostra SJ32_837.1

Number	$^{207}Pb^{a}$ (cps)	U^{b} (ppm)	Pb^{b} (ppm)	$\frac{Th}{U}^{b}$	$\frac{^{206}Pb}{^{204}Pb}$	$\frac{^{206}Pb^{c}}{^{238}U}$	2 σ %	$\frac{^{207}Pb^{c}}{^{235}U}$	2 σ %	$\frac{^{207}Pb^{c}}{^{206}Pb}$	2 σ %	rho[d]	$\frac{^{206}Pb}{^{238}U}$	2 σ (Ma)	$\frac{^{207}Pb}{^{235}U}$	2 σ (Ma)	$\frac{^{207}Pb}{^{206}Pb}$	2 σ (Ma)	conc %
A-5	6230	282	16	0.33	1	0.05688	3.5	0.47420	7.0	0.06048	6.0	0.51	357	12	394	23	620	130	57
A-6	8226	419	24	0.53	0	0.05706	3.4	0.46290	6.5	0.05885	5.5	0.53	358	12	386	21	561	120	64
A-7	12202	548	30	0.19	0	0.05492	3.7	0.46790	5.3	0.06180	3.8	0.69	345	12	390	17	667	82	52
A-8	12311	540	30	0.64	0	0.05725	3.6	0.43770	6.3	0.05546	5.2	0.56	359	12	369	19	430	116	83
A-9	12444	574	31	0.18	0	0.05473	3.5	0.40360	4.8	0.05350	3.3	0.73	343	12	344	14	349	74	**98**
A-10	6941	265	15	0.36	1	0.05614	3.7	0.46450	5.3	0.06002	3.7	0.71	352	13	387	17	604	81	58
A-11	11980	478	25	1.04	1	0.05282	3.8	0.43380	5.9	0.05959	4.6	0.63	332	12	366	18	588	100	56
A-13	5615	220	13	0.67	0	0.06175	3.4	0.46650	6.4	0.05481	5.4	0.53	386	13	389	21	404	121	**96**
A-14	8790	402	23	0.16	b.d.	0.05898	3.7	0.50520	5.3	0.06214	3.8	0.69	369	13	415	18	678	82	54
A-15	24639	971	60	2.53	0	0.06280	3.6	0.47830	4.5	0.05526	2.7	0.80	393	14	397	15	422	60	**93**
A-16	7982	352	18	0.25	0	0.05285	3.8	0.40100	5.1	0.05505	3.3	0.75	332	12	342	15	413	75	80
A-17	22745	911	54	1.30	0	0.05974	3.3	0.44530	4.2	0.05407	2.5	0.79	374	12	374	13	373	57	**100**
A-18	15908	707	40	0.20	0	0.05694	3.2	0.42070	4.3	0.05360	2.8	0.75	357	11	357	13	354	64	**101**
A-19	10188	465	22	0.38	1	0.04777	3.4	0.36040	5.1	0.05473	3.9	0.65	301	10	313	14	401	87	75
A-20	16971	663	39	0.67	b.d.	0.05882	3.7	0.51440	4.8	0.06345	3.0	0.77	368	13	421	16	723	65	51
A-21	13863	319	31	0.28	b.d.	0.09857	3.3	0.82500	4.1	0.06072	2.3	0.82	606	19	611	19	629	50	**96**
A-22	12700	561	35	0.26	0	0.06335	3.5	0.47760	4.8	0.05469	3.2	0.74	396	14	396	16	399	71	**99**
A-23	22708	886	50	0.41	0	0.05683	3.6	0.47600	4.6	0.06076	2.9	0.78	356	12	395	15	630	63	57
A-24	2709	104	7	0.64	0	0.06502	4.0	0.49430	8.0	0.05516	7.0	0.49	406	16	408	27	418	156	**97**
A-29	19030	650	35	0.53	0	0.05330	3.5	0.55930	6.9	0.07613	5.9	0.51	335	11	451	25	1098	118	30
A-30	13271	603	42	0.38	b.d.	0.06957	3.8	0.60100	5.3	0.06268	3.7	0.72	434	16	478	20	697	78	62
A-31	54119	103	51	0.50	0	0.46060	3.8	10.11000	4.4	0.15920	2.3	0.85	2442	77	2445	41	2447	39	**100**
A-32	3284	21	5	1.10	1	0.22600	4.0	2.65400	8.2	0.08521	7.2	0.49	1313	48	1316	61	1320	139	**100**
A-33	15665	659	37	0.94	0	0.05632	3.4	0.43290	4.0	0.05577	2.2	0.84	353	12	365	12	442	48	80
A-34	4477	171	10	0.34	0	0.06028	3.9	0.46750	7.0	0.05627	5.9	0.55	377	14	389	23	462	131	82
A-35	7130	321	17	0.25	0	0.05476	4.0	0.40170	5.6	0.05322	3.8	0.73	344	14	343	16	337	87	**102**
A-36	5816	225	12	0.90	0	0.05531	3.9	0.40550	7.4	0.05319	6.3	0.53	347	13	346	22	336	143	**103**
A-37	9540	541	31	0.38	1	0.05799	3.8	0.43050	5.4	0.05386	3.9	0.70	363	13	364	17	365	88	**100**
A-38	3784	216	12	0.91	1	0.05747	3.8	0.42870	7.6	0.05412	6.6	0.49	360	13	362	23	375	149	**96**
A-39	28401	1181	73	0.25	0	0.06319	3.4	0.47400	4.0	0.05442	2.1	0.85	395	13	394	13	388	48	**102**
A-40	9855	426	23	0.23	0	0.05508	3.5	0.40440	5.1	0.05327	3.8	0.68	346	12	345	15	340	86	**102**
A-41	15572	665	39	1.31	0	0.06024	3.6	0.45260	4.7	0.05451	3.0	0.77	377	13	379	15	391	67	**96**
A-42	7941	345	17	1.11	0	0.05034	4.0	0.39720	5.9	0.05725	4.4	0.67	317	12	340	17	500	96	63
A-43	19629	835	49	0.27	0	0.06016	3.2	0.44870	4.4	0.05412	2.9	0.75	377	12	376	14	375	65	**100**
A-44	5654	247	13	0.79	0	0.05179	3.6	0.39650	5.6	0.05554	4.3	0.64	325	11	339	16	433	95	75
A-45	20972	822	47	0.56	0	0.05773	3.4	0.48290	4.9	0.06068	3.6	0.69	362	12	400	16	627	77	58
A-46	96962	470	99	0.32	1	0.19780	3.5	3.91300	3.8	0.14350	1.6	0.91	1164	37	1616	31	2269	28	51
A-47	11252	515	28	0.80	0	0.05478	3.6	0.40960	5.7	0.05424	4.4	0.64	344	12	349	17	380	98	**90**
A-48	11639	406	21	0.25	2	0.05318	3.6	0.44280	7.3	0.06041	6.4	0.49	334	12	372	23	618	137	54
A-53	15668	667	39	0.21	0	0.05972	4.1	0.44920	5.3	0.05457	3.4	0.77	374	15	377	17	394	75	**95**
A-54	12801	609	34	0.95	1	0.05661	3.7	0.41720	4.9	0.05346	3.3	0.74	355	13	354	15	348	74	**102**
A-55	7136	306	17	0.44	0	0.05576	3.6	0.41420	5.9	0.05389	4.7	0.61	350	12	352	18	366	107	**96**
A-56	14404	640	40	1.42	0	0.06417	3.4	0.50220	4.5	0.05678	3.0	0.75	401	13	413	15	482	65	83
A-57	18172	767	45	0.47	0	0.05973	3.8	0.48320	5.3	0.05869	3.6	0.73	374	14	400	17	555	79	67
A-58	14023	593	35	0.22	1	0.05971	4.5	0.44640	9.2	0.05424	8.0	0.49	374	16	375	29	380	181	**98**
A-59	43800	1267	75	1.42	2	0.05998	3.4	0.53220	5.7	0.06437	4.6	0.59	376	12	433	20	753	97	50
A-60	17391	805	47	0.53	b.d.	0.05909	3.3	0.43630	4.1	0.05356	2.5	0.80	370	12	368	13	352	57	**105**
A-61	16449	732	42	0.17	0	0.05829	3.3	0.43420	4.4	0.05404	2.9	0.75	365	12	366	14	372	66	**98**
A-62	10172	505	26	0.22	0	0.05154	3.4	0.38500	4.9	0.05420	3.5	0.70	324	11	331	14	379	79	86
A-63	62743	2775	161	2.10	0	0.05904	3.3	0.45280	3.6	0.05564	1.4	0.92	370	12	379	11	437	32	85
A-64	9623	429	23	1.31	0	0.05495	4.2	0.44480	5.6	0.05873	3.7	0.75	345	14	374	18	556	81	62
A-77	10945	541	29	0.39	0	0.05541	3.9	0.40870	5.7	0.05350	4.1	0.68	348	13	348	17	350	93	**99**
A-78	9191	420	24	0.26	1	0.05734	3.6	0.42140	5.7	0.05331	4.4	0.63	359	13	357	17	341	100	**105**
A-79	22366	1052	61	0.24	0	0.05858	3.7	0.43410	4.4	0.05377	2.5	0.83	367	13	366	14	361	56	**102**
A-80	19818	915	51	1.43	0	0.05654	3.5	0.46220	4.6	0.05930	2.9	0.77	355	12	386	15	577	63	61
A-82	4296	170	10	0.82	2	0.06102	3.5	0.46040	10.4	0.05474	9.8	0.34	382	13	385	33	401	219	**95**
A-83	4401	197	11	0.50	0	0.05494	4.0	0.40470	7.3	0.05345	6.1	0.55	345	13	345	21	347	138	**99**
A-84	13665	679	40	0.73	0	0.05964	3.6	0.44420	5.0	0.05403	3.4	0.73	373	13	373	15	372	77	**101**
A-85	7648	350	21	0.95	b.d.	0.06114	3.5	0.62650	5.2	0.07433	3.8	0.68	383	13	494	20	1050	77	36
A-86	17170	768	46	0.35	0	0.06023	3.4	0.46260	4.6	0.05573	3.1	0.74	377	13	386	15	441	70	86
A-87	10623	530	29	0.13	0	0.05480	3.7	0.40300	4.9	0.05335	3.3	0.75	344	12	344	14	343	74	**100**
A-88	15611	713	44	0.18	0	0.06308	3.4	0.47340	4.3	0.05444	2.6	0.79	394	13	394	14	389	59	**101**
A-89	17935	843	50	0.18	0	0.06078	3.4	0.45290	4.0	0.05405	2.1	0.85	380	13	379	13	373	48	**102**
A-90	3176	147	9	0.59	0	0.05996	4.0	0.45160	6.4	0.05464	5.0	0.62	375	15	378	20	397	112	**95**
A-91	28646	551	50	0.20	5	0.08926	6.0	1.23800	26.3	0.10060	25.6	0.23	551	32	818	148	1635	476	34
A-92	17447	776	49	0.40	1	0.06389	4.3	0.48170	4.9	0.05470	2.3	0.88	399	17	399	16	400	52	**100**
A-93	10878	525	28	0.64	1	0.05489	3.7	0.38410	7.8	0.05076	6.8	0.48	344	13	330	22	229	158	150
A-94	7315	361	21	0.15	0	0.05974	3.5	0.44700	6.0	0.05429	4.8	0.58	374	13	375	19	382	109	**98**
A-95	57351	377	78	0.21	0	0.20080	3.9	2.97100	4.5	0.10730	2.2	0.86	1180	42	1400	34	1754	41	67
A-96	2943	115	7	0.75	1	0.05927	3.5	0.48150	8.0	0.05894	7.2	0.43	371	13	399	26	564	157	66
A-101	13333	498	28	0.13	2	0.05619	3.5	0.41160	5.6	0.05314	4.4	0.62	352	12	350	17	334	99	**105**
A-102	15367	709	31	2.87	1	0.04464	3.5	0.35480	6.7	0.05766	5.7	0.52	282	10	308	18	516	126	55
A-103	41297	1197	69	0.62	3	0.05815	3.5	0.46390	6.2	0.05788	5.1	0.56	364	12	387	20	525	112	69
A-104	14873	750	44	0.72	0	0.06025	3.4	0.45070	5.0	0.05427	3.7	0.68	377	12	378	16	382	82	**99**
A-105	7644	350	20	0.61	1	0.05825	3.7	0.45650	6.6	0.05686	5.4	0.57	365	13	382	21	486	119	75
A-106	15032	991	62	0.19	0	0.06381	3.7	0.47900	5.0	0.05446	3.3	0.74	399	14	397	16	389	75	**102**
A-107	1901	112	6	0.70	1	0.05631	7.0	0.41960	15.6	0.05406	13.9	0.45	353	24	356	47	373	313	**95**
A-108	12470	689	35	0.18	0	0.05205	3.4	0.43300	4.5	0.06035	2.9	0.76	327	11	365	14	616	63	53
A-109	13908	703	48	0.16	b.d.	0.06963	3.6	0.58330	4.5	0.06077	2.6	0.82	434	15	467	17	631	56	69
A-110	28693	1143	73	0.96	0	0.06478	3.4	0.54810	4.5	0.06138	3.0	0.74	405	13	444	16	652	65	62
A-111	17503	846	50	0.21	0	0.05969	3.6	0.44940	4.4	0.05462	2.6	0.80	374	13	377	14	396	59	**94**
A-112	14599	746	48	0.92	0	0.06580	3.4	0.52380	4.7	0.05775	3.2	0.72	411	13	428	16	520	71	79
A-113	11248	625	33	0.29	0	0.05434	3.5	0.39820	4.8	0.05315	3.4	0.72	341	12	340	14	335	76	**102**
A-114	16693	812	49	0.24	0	0.06108	3.8	0.45640	4.6	0.05422	2.5	0.83	382	14	382	14	379	56	**101**
A-115	27666	1254	75	1.30	0	0.06091	3.3	0.49250	3.9	0.05866	2.1	0.84	381	12	407	13	554	46	69
A-116	19228	759	50	0.24	2	0.06641	4.2	0.50340	10.2	0.05500	9.3	0.41	414	17	414	35	411	208	**101**
A-117	9377	450	25	0.17	1	0.05576	3.5	0.41090	6.5	0.05346	5.5	0.54	350	12	349	19	348	123	**101**
A-118	19788	1006	55	0.27	0	0.05599	3.2	0.41650	4.2	0.05396	2.7	0.77	351	11	354	12	369	60	**95**
A-119	11337	581	31	1.38	2	0.05400	3.4	0.48980	9.3	0.06580	8.7	0.37	339	11	405	31	799	182	42
A-120	8038	432	24	1.25	0	0.05740	3.3	0.42640	5.0	0.05389	3.8	0.66	360	12	361	15	366	85	**98**

Sample PSK50B_1043.7
Amostra PSK50B_1043.7

Number	$^{207}Pb^a$ (cps)	U^b (ppm)	Pb^b (ppm)	$\frac{Th^b}{U}$	$\frac{^{206}Pb}{^{204}Pb}$	$\frac{^{206}Pb^c}{^{238}U}$	2 σ %	$\frac{^{207}Pb^c}{^{235}U}$	2 σ %	$\frac{^{207}Pb^c}{^{206}Pb}$	2 σ %	rho^d	$\frac{^{206}Pb}{^{238}U}$	2 σ (Ma)	$\frac{^{207}Pb}{^{235}U}$	2 σ (Ma)	$\frac{^{207}Pb}{^{206}Pb}$	2 σ (Ma)	conc %
A-85	5596	236	13	0.36	0	0.05639	3.4	0.43400	5.2	0.05583	3.9	0.65	354	12	366	16	445	87	79
A-86	5243	225	12	0.44	0	0.05544	3.4	0.41990	6.9	0.05495	6.0	0.50	348	12	356	21	409	134	85
A-87	5180	198	11	0.35	1	0.05691	3.3	0.43940	5.0	0.05600	3.8	0.65	357	11	370	16	452	85	79
A-88	17571	758	44	0.29	0	0.05919	3.2	0.43780	4.0	0.05366	2.3	0.81	371	12	369	12	356	52	**104**
A-89	10731	463	24	0.21	1	0.05269	3.3	0.38840	4.9	0.05348	3.7	0.66	331	11	333	14	349	83	**95**
A-90	52659	1165	64	0.58	4	0.05468	3.3	0.59440	5.3	0.07886	4.1	0.64	343	11	474	20	1168	80	29
A-91	22229	948	53	0.57	0	0.05623	3.2	0.43290	3.9	0.05586	2.3	0.82	353	11	365	12	446	50	79
A-92	20390	744	41	0.47	b.d.	0.05482	3.2	0.50850	3.6	0.06730	1.7	0.89	344	11	417	12	846	35	41
A-93	7433	341	17	0.18	0	0.05140	3.2	0.38030	4.6	0.05369	3.3	0.69	323	10	327	13	357	75	**90**
A-94	19861	827	48	0.25	0	0.05818	3.1	0.47080	3.7	0.05871	2.1	0.82	365	11	392	12	556	46	66
A-95	6756	305	17	0.49	0	0.05573	3.2	0.41260	4.5	0.05371	3.2	0.71	350	11	351	13	358	72	**98**
A-96	15943	632	34	1.36	0	0.05443	3.4	0.51100	5.6	0.06811	4.5	0.61	342	11	419	19	871	92	39
A-97	17611	786	43	0.18	0	0.05560	3.2	0.41200	4.2	0.05375	2.7	0.77	349	11	350	12	360	61	**97**
A-98	25051	754	36	0.91	0	0.04682	3.5	0.68030	4.6	0.10540	3.0	0.76	295	10	527	19	1721	55	17
A-99	13568	595	29	0.27	1	0.04904	3.3	0.36820	4.5	0.05448	3.1	0.73	309	10	318	12	390	69	79
A-100	6735	285	15	0.26	0	0.05480	3.2	0.42180	6.1	0.05584	5.2	0.53	344	11	357	18	445	115	77
A-106	9947	468	23	0.37	0	0.04988	3.2	0.38130	5.0	0.05546	3.8	0.65	314	10	328	14	430	84	73
A-107	24888	105	33	0.73	0	0.30170	3.2	4.51500	3.8	0.10860	2.0	0.85	1700	48	1734	31	1775	36	**96**
A-108	11460	519	26	0.40	0	0.05129	3.2	0.41080	4.4	0.05812	2.9	0.74	322	10	349	13	534	64	60
A-109	6113	260	14	0.42	0	0.05570	3.3	0.41710	5.3	0.05433	4.2	0.61	349	11	354	16	384	95	**91**
A-110	6322	286	16	0.29	0	0.05541	3.3	0.41210	4.9	0.05395	3.7	0.67	348	11	350	15	368	83	**94**
A-111	15095	693	40	0.24	0	0.05884	3.3	0.43830	4.0	0.05404	2.4	0.81	369	12	369	12	372	53	**99**
A-112	11770	600	29	0.38	0	0.04980	3.3	0.35900	4.8	0.05231	3.5	0.68	313	10	311	13	298	79	**105**
A-113	4769	214	12	0.23	0	0.05661	3.4	0.41620	6.2	0.05334	5.2	0.55	355	12	353	19	343	118	**104**
A-114	16157	725	42	0.31	0	0.05854	3.2	0.44940	4.2	0.05570	2.6	0.78	367	12	377	13	440	58	83
A-115	6677	284	15	0.15	0	0.05479	3.5	0.41990	5.4	0.05560	4.1	0.65	344	12	356	16	436	92	79
A-116	32836	1065	59	0.24	2	0.05567	3.2	0.45580	4.6	0.05940	3.3	0.70	349	11	381	15	581	71	60
A-117	12771	522	27	0.33	1	0.05227	3.3	0.43510	4.9	0.06040	3.6	0.68	328	11	367	15	617	78	53
A-118	15115	483	22	1.18	0	0.04475	3.4	0.52800	4.6	0.08560	3.1	0.74	282	9	431	16	1329	59	21
A-119	26039	1032	55	0.99	b.d.	0.05297	3.1	0.51380	3.7	0.07037	2.1	0.83	333	10	421	13	939	42	35
A-120	9602	483	26	0.35	0	0.05437	3.2	0.40360	5.2	0.05385	4.0	0.62	341	11	344	15	364	91	**94**
A-121	16034	522	28	0.79	0	0.05430	3.3	0.58080	4.9	0.07761	3.6	0.67	341	11	465	18	1136	72	30
A-122	10562	544	28	0.80	0	0.05282	3.2	0.38700	4.4	0.05314	3.0	0.72	332	10	332	12	334	69	**99**
A-123	6028	281	15	0.76	1	0.05386	3.2	0.39190	6.1	0.05279	5.2	0.52	338	10	336	17	319	119	**106**
A-124	18688	714	42	0.25	2	0.06026	3.5	0.47960	4.4	0.05774	2.7	0.79	377	13	398	15	519	60	73
A-125	13350	690	39	0.22	0	0.05747	3.3	0.42360	4.3	0.05347	2.7	0.78	360	12	359	13	348	61	**103**
A-131	10893	558	27	0.56	0	0.04974	3.4	0.39290	4.8	0.05731	3.3	0.72	313	10	336	14	503	73	62
A-132	21961	697	39	0.54	3	0.05595	3.4	0.54360	4.9	0.07049	3.5	0.70	351	12	441	17	942	72	37
A-133	10671	145	9	0.78	10	0.05994	3.7	0.62410	10.9	0.07554	10.2	0.34	375	14	492	42	1082	204	35
A-134	10032	512	26	0.36	0	0.05077	3.3	0.39460	6.0	0.05639	5.0	0.56	319	10	338	17	467	110	68
A-135	16354	789	44	0.28	0	0.05677	3.3	0.41990	4.0	0.05366	2.2	0.83	356	12	356	12	356	51	**100**
A-136	35501	795	47	0.65	7	0.05897	3.6	0.69430	6.7	0.08542	5.7	0.53	369	13	535	28	1325	110	28
A-137	9588	452	23	0.23	1	0.05119	3.3	0.37820	5.0	0.05359	3.7	0.66	322	10	326	14	353	85	**91**
A-138	5559	276	15	0.22	0	0.05616	3.3	0.41630	5.9	0.05378	4.9	0.56	352	11	353	18	361	110	**97**
A-139	20868	888	49	0.42	0	0.05566	3.2	0.47780	4.0	0.06227	2.3	0.81	349	11	397	13	683	49	51
A-140	25400	977	55	1.12	1	0.05638	3.4	0.49530	4.5	0.06373	3.0	0.74	354	12	409	15	732	64	48
A-141	8325	378	20	0.73	0	0.05352	3.2	0.51330	7.6	0.06958	6.9	0.42	336	10	421	26	915	143	37
A-142	32199	954	54	0.25	4	0.05710	3.1	0.45790	4.6	0.05818	3.4	0.67	358	11	383	15	536	74	67
A-143	9867	506	25	0.12	0	0.04932	3.3	0.36510	4.9	0.05371	3.7	0.67	310	10	316	13	358	83	87
A-144	23969	959	54	0.36	0	0.05666	3.2	0.52050	4.2	0.06665	2.7	0.76	355	11	425	15	826	56	43
A-145	12010	608	31	0.19	1	0.05127	3.3	0.37350	5.1	0.05285	3.9	0.64	322	10	322	14	322	88	**100**
A-146	25328	1021	56	0.28	2	0.05583	3.2	0.45970	4.7	0.05974	3.4	0.69	350	11	384	15	593	74	59
A-147	12138	548	25	0.69	1	0.04654	3.4	0.39710	5.8	0.06191	4.7	0.59	293	10	340	17	670	100	44
A-148	10638	594	29	0.21	0	0.05043	3.3	0.37340	4.6	0.05372	3.3	0.70	317	10	322	13	359	75	88

Sample MM09001_486.6
Amostra MM09001_486.6

Number	^{207}Pb (cps)	U^a (ppm)	Pb^a (ppm)	Th^c U	^{206}Pb ^{204}Pb	$^{206}Pb^e$ ^{238}U	2 σ %	$^{207}Pb^e$ ^{235}U	2 σ %	$^{207}Pb^e$ ^{206}Pb	2 σ %	rho	^{206}Pb ^{238}U	2 σ (Ma)	^{207}Pb ^{235}U	2 σ (Ma)	^{207}Pb ^{206}Pb	2 σ (Ma)	conc %
a1	14361	649	37	0.10	15921	0.05945	2.1	0.44476	2.5	0.05426	1.4	0.83	372	8	374	8	382	31	**97**
a2	45686	444	48	0.71	18199	0.06833	12.0	2.28254	22.1	0.24229	18.5	0.54	426	50	1207	169	3135	295	14
a3	10457	479	26	0.13	9192	0.05507	2.0	0.41574	2.6	0.05475	1.7	0.76	346	7	353	8	402	38	86
a4	10810	488	28	0.12	20240	0.06030	2.4	0.44732	3.0	0.05380	1.8	0.80	377	9	375	9	363	40	**104**
a5	15670	426	46	0.71	26287	0.09039	1.6	0.74820	2.2	0.06003	1.4	0.76	558	9	567	9	605	30	**92**
a6	15440	657	40	0.36	2987	0.05917	1.8	0.48940	2.6	0.05999	1.9	0.67	371	6	405	9	603	42	61
a7	16113	886	43	0.12	2018	0.04073	1.9	0.35897	2.8	0.06392	2.0	0.68	257	5	311	7	739	43	35
a8	15390	703	42	0.37	3474	0.05818	1.9	0.46181	2.9	0.05757	2.2	0.65	365	7	386	9	513	49	71
a9	14610	668	39	0.53	2864	0.05631	2.1	0.44572	3.1	0.05741	2.2	0.70	353	7	374	10	507	48	70
a10	12989	506	29	0.16	1288	0.05693	1.8	0.51793	3.4	0.06598	2.9	0.52	357	6	424	12	806	61	44
a11	7130	282	11	0.61	2738	0.02830	9.0	0.26324	10.7	0.06747	5.8	0.84	180	16	237	23	852	121	21
a12	17845	860	44	0.14	2062	0.05205	2.1	0.42260	2.7	0.05888	1.7	0.77	327	7	358	8	563	38	58
a13	19169	779	50	0.57	5733	0.05671	1.9	0.45565	2.6	0.05827	1.8	0.72	356	7	381	8	540	40	66
a14	12846	571	34	0.17	6646	0.06073	1.9	0.46631	3.1	0.05569	2.4	0.62	380	7	389	10	440	54	86
a15	15562	732	40	0.24	4662	0.05517	2.1	0.43319	3.4	0.05695	2.7	0.62	346	7	365	10	490	59	71
a16	10168	490	28	0.13	19059	0.05883	2.1	0.43722	3.4	0.05390	2.6	0.63	369	8	368	10	367	59	**100**
a17	11672	491	32	0.42	4275	0.05929	1.8	0.48317	3.0	0.05911	2.4	0.59	371	6	400	10	571	52	65
a18	10361	482	28	0.28	5437	0.05646	1.7	0.44775	2.9	0.05751	2.4	0.58	354	6	376	9	511	52	69
a19	8362	371	23	0.44	4020	0.05713	2.1	0.45157	3.2	0.05733	2.4	0.65	358	7	378	10	504	53	71
a20	24910	1194	79	0.07	1808	0.05782	2.1	0.43014	5.2	0.05396	4.8	0.41	362	8	363	16	369	107	**98**
a21	9706	444	26	0.14	9779	0.05929	1.7	0.44829	2.7	0.05483	2.1	0.64	371	6	376	9	405	47	**92**
a22	15049	690	41	0.30	6294	0.05696	1.7	0.43977	2.6	0.05600	1.9	0.67	357	6	370	8	452	42	79
a23	7724	277	17	0.24	1181	0.05772	1.9	0.52196	4.0	0.06558	3.5	0.47	362	7	426	14	793	74	46
a24	11806	468	27	0.20	1446	0.05677	2.0	0.51123	3.0	0.06531	2.2	0.68	356	7	419	10	784	47	45
a25	11725	502	28	0.18	20827	0.05491	2.0	0.42873	3.1	0.05663	2.4	0.65	345	7	362	10	477	52	72
a26	27225	696	46	0.45	391	0.05398	2.1	0.68551	7.2	0.09211	6.9	0.29	339	7	530	30	1470	130	23
a27	14996	716	40	0.29	27998	0.05751	1.8	0.42831	2.6	0.05401	1.9	0.69	360	6	362	8	372	42	**97**
a28	65064	689	90	0.34	121	0.08630	2.6	2.09103	6.4	0.17573	5.8	0.41	534	14	1146	45	2613	96	20
a29	9813	471	26	0.38	3647	0.05418	1.8	0.43700	2.9	0.05850	2.3	0.62	340	6	368	9	548	50	62
a30	13445	602	34	0.16	9580	0.05825	1.8	0.44071	2.4	0.05488	1.5	0.77	365	7	371	7	407	35	90
a31	12387	546	30	0.18	1532	0.05508	2.1	0.46299	4.0	0.06096	3.4	0.53	346	7	386	13	638	72	54
a32	24898	1359	70	0.06	8257	0.04571	2.2	0.35575	3.0	0.05644	2.0	0.74	288	6	309	8	470	45	61
a33	2650	124	8	0.42	4955	0.05847	2.1	0.43515	4.3	0.05398	3.8	0.48	366	7	367	13	370	85	**99**
a34	6183	287	19	0.59	11494	0.05753	1.7	0.43149	3.5	0.05440	3.0	0.49	361	6	364	11	388	68	**93**
a35	11035	574	33	0.50	1781	0.05637	2.2	0.47435	3.3	0.06104	2.5	0.65	353	7	394	11	640	55	55
a36	12301	550	31	0.13	4223	0.05922	1.8	0.44222	2.5	0.05416	1.7	0.72	371	6	372	8	378	39	**98**
a37	16745	760	42	0.21	6453	0.05677	1.7	0.43276	2.4	0.05529	1.7	0.71	356	6	365	8	424	38	84
a38	5809	246	16	0.36	5703	0.06117	1.7	0.45766	2.7	0.05426	2.1	0.63	383	6	383	9	382	47	**100**
a39	14878	679	40	0.29	8155	0.05802	1.8	0.44392	2.4	0.05549	1.6	0.74	364	6	373	7	432	36	84
a40	9013	415	23	0.07	16817	0.05861	1.9	0.43667	2.5	0.05404	1.7	0.74	367	7	368	8	373	38	**99**
a41	14532	666	39	0.15	6389	0.06023	1.8	0.45341	2.2	0.05460	1.1	0.85	377	7	380	7	396	25	**95**
a42	#DIV/0!	#DIV/0!	#DIV/0!	######	#DIV/0!	0.00000	#####	#DIV/0!	######	#DIV/0!	######	######	0	######	#VALUE!	######	#VALUE!	#######	######
a43	6995	302	15	1.17	309	0.03748	3.0	0.53552	6.0	0.10363	5.2	0.50	237	7	435	21	1690	96	14
a44	13369	621	35	0.12	6918	0.05874	1.9	0.44537	2.5	0.05499	1.6	0.78	368	7	374	8	412	35	89
a45	14358	690	41	0.29	6306	0.05834	1.7	0.44089	2.5	0.05481	1.8	0.70	365	6	371	8	405	39	**90**
a46	16121	764	44	0.12	16054	0.06095	1.7	0.45417	2.3	0.05404	1.5	0.76	381	6	380	7	373	34	**102**
a47	14439	645	43	0.63	3711	0.05786	1.8	0.46366	2.7	0.05812	2.0	0.67	363	6	387	9	534	43	68
a48	5596	278	18	0.36	10345	0.06156	2.3	0.46243	3.3	0.05448	2.3	0.72	385	9	386	10	391	51	**99**
a49	13939	653	39	0.44	4624	0.05556	2.0	0.42803	3.4	0.05587	2.7	0.60	349	7	362	10	447	60	78
a50	10923	498	29	0.14	6856	0.06134	1.9	0.46608	2.7	0.05511	1.9	0.72	384	7	388	9	417	41	**92**
a51	11329	526	31	0.14	21363	0.06174	1.8	0.45531	2.4	0.05349	1.6	0.75	386	7	381	8	350	36	110
a52	24394	1177	65	0.20	1824	0.04877	2.1	0.38811	2.5	0.05772	1.4	0.83	307	6	333	7	519	31	59
a53	9961	470	31	0.45	18565	0.06073	1.6	0.45271	2.6	0.05407	2.0	0.64	380	6	379	8	374	44	**102**
a54	13250	627	35	0.15	3633	0.05862	2.2	0.44279	2.6	0.05478	1.3	0.85	367	8	372	8	403	30	**91**
a55	8662	415	24	0.25	11083	0.05645	1.7	0.43051	2.7	0.05531	2.1	0.64	354	6	364	8	425	47	83
a56	21734	1126	50	0.19	2641	0.04368	1.8	0.38735	2.6	0.06432	1.9	0.69	276	5	332	7	752	39	37
a57	14670	672	39	0.15	8462	0.05959	1.7	0.44813	2.4	0.05454	1.7	0.72	373	6	376	8	393	38	**95**
a58	12415	673	43	0.34	23212	0.06168	2.7	0.45804	3.1	0.05386	1.5	0.87	386	10	383	10	365	34	**106**
a59	14365	605	23	0.40	739	0.03367	3.1	0.33254	6.0	0.07163	5.1	0.52	213	7	292	15	975	104	22
a60	12893	637	38	0.27	20270	0.05899	1.8	0.44002	2.2	0.05410	1.4	0.80	369	6	370	7	375	31	**98**
a61	16973	548	51	0.23	29153	0.09405	1.8	0.75892	2.4	0.05853	1.6	0.75	579	10	573	11	550	35	**105**
a62	33454	758	59	0.08	716	0.07776	2.0	0.62872	3.5	0.05864	2.8	0.59	483	10	495	14	554	61	87
a63	19873	808	45	0.14	488	0.05342	1.8	0.57754	3.2	0.07841	2.6	0.58	336	6	463	12	1157	51	29
a64	19614	892	53	0.25	2817	0.06122	2.1	0.47904	2.6	0.05675	1.5	0.81	383	8	397	8	482	33	80
a65	5214	284	14	0.53	9638	0.04485	2.1	0.33743	3.9	0.05456	3.3	0.54	283	6	295	10	394	73	72
a66	9080	411	26	0.08	15568	0.06346	1.8	0.48037	5.1	0.05490	4.8	0.35	397	7	398	17	408	108	**97**
a67	8923	422	26	0.51	1874	0.05590	1.9	0.45955	6.1	0.05962	5.8	0.31	351	7	384	20	590	126	59
a68	12987	473	41	0.18	789	0.05180	2.0	0.53666	5.6	0.07514	5.2	0.37	326	6	436	20	1072	104	30
a69	20043	516	39	0.66	1	0.05857	2.7	0.97807	24.7	0.12111	24.5	0.11	367	10	693	132	1973	437	19
a70	12207	375	23	0.31	445	0.05358	2.1	0.63379	3.3	0.08579	2.5	0.63	336	7	498	13	1334	49	25

Sample MM09001_486.6 (cont.)
Amostra MM09001_486.6 (cont.)

Number	^{207}Pb (cps)	U^a (ppm)	Pb^a (ppm)	$\frac{Th^c}{U}$	$\frac{^{206}Pb}{^{204}Pb}$	$\frac{^{206}Pb^e}{^{238}U}$	2 σ %	$\frac{^{207}Pb^e}{^{235}U}$	2 σ %	$\frac{^{207}Pb^e}{^{206}Pb}$	2 σ %	rho	$\frac{^{206}Pb}{^{238}U}$	2 σ (Ma)	$\frac{^{207}Pb}{^{235}U}$	2 σ (Ma)	$\frac{^{207}Pb}{^{206}Pb}$	2 σ (Ma)	conc %
a71	12384	644	37	0.29	22920	0.05577	1.7	0.41913	2.6	0.05451	1.9	0.68	350	6	355	8	392	43	89
a72	11316	462	33	0.84	1515	0.05927	1.8	0.55358	5.2	0.06773	4.9	0.35	371	7	447	19	860	102	43
a73	16342	745	43	0.40	1449	0.05071	2.7	0.42519	3.3	0.06081	1.9	0.82	319	8	360	10	633	41	50
a74	14575	724	41	0.25	27191	0.05578	1.8	0.41545	2.2	0.05402	1.2	0.83	350	6	353	7	372	27	**94**
a75	13985	327	23	0.35	398	0.05743	2.6	0.78029	16.1	0.09855	15.9	0.16	360	9	586	74	1597	297	23
a76	5141	251	15	0.28	9572	0.05883	2.3	0.43955	3.5	0.05419	2.6	0.65	368	8	370	11	379	59	**97**
a77	15869	758	41	0.17	2677	0.05536	1.8	0.43684	2.7	0.05723	2.0	0.65	347	6	368	8	500	45	69
a78	17752	871	50	0.50	3083	0.05177	2.0	0.42312	3.2	0.05928	2.4	0.64	325	6	358	10	577	53	56
a79	10950	516	30	0.19	7361	0.05942	1.9	0.44422	3.4	0.05422	2.8	0.56	372	7	373	11	380	63	**98**
a80	13403	599	37	0.39	5791	0.05762	1.8	0.44678	2.7	0.05624	2.0	0.68	361	6	375	9	462	44	78
a81	7861	364	21	0.16	7619	0.05858	2.1	0.44204	2.8	0.05473	1.8	0.74	367	7	372	9	401	41	**91**
a82	9318	460	26	0.21	11533	0.05789	1.9	0.42958	2.7	0.05382	2.0	0.69	363	7	363	8	364	45	**100**
a83	8333	387	22	0.15	15419	0.05839	1.9	0.43874	3.4	0.05450	2.8	0.57	366	7	369	11	392	62	**93**
a84	15118	710	40	0.28	5051	0.05520	1.8	0.41707	2.5	0.05480	1.8	0.72	346	6	354	8	404	39	86
a85	17690	1424	48	0.10	1791	0.02491	4.5	0.20387	4.7	0.05935	1.1	0.97	159	7	188	8	580	25	27
a86	10513	532	30	0.20	19425	0.05579	2.1	0.42082	2.9	0.05471	1.9	0.73	350	7	357	9	400	43	87
a87	8910	1064	27	0.09	708	0.02440	1.8	0.19106	3.7	0.05680	3.3	0.48	155	3	178	6	484	72	32
a88	12816	646	37	0.21	7861	0.05759	1.7	0.42858	2.6	0.05397	1.9	0.67	361	6	362	8	370	43	**98**
a89	16083	791	44	0.17	25437	0.05712	1.8	0.42836	2.4	0.05439	1.6	0.74	358	6	362	7	387	37	**93**
a90	11127	506	29	0.30	2362	0.05488	1.7	0.42594	2.8	0.05629	2.3	0.59	344	6	360	9	464	51	74
a91	11866	657	33	0.30	19317	0.05170	2.0	0.39625	2.7	0.05558	1.8	0.74	325	6	339	8	436	41	75
a92	9074	453	26	0.27	16781	0.05661	1.8	0.42538	2.9	0.05450	2.2	0.64	355	6	360	9	392	50	**91**
a93	8143	409	26	0.44	15128	0.05884	1.7	0.44044	2.3	0.05429	1.6	0.72	369	6	371	7	383	36	**96**
a94	13261	538	38	0.61	1896	0.06063	1.8	0.53709	2.8	0.06425	2.1	0.65	379	7	437	10	750	45	51
a95	7063	335	19	0.12	13009	0.05758	1.7	0.43427	2.6	0.05470	2.0	0.64	361	6	366	8	400	45	**90**
a96	9964	376	25	0.90	479	0.05223	2.0	0.50073	7.1	0.06953	6.8	0.29	328	7	412	24	915	140	36
a97	13192	614	49	0.72	20067	0.06455	1.7	0.48280	2.7	0.05425	2.1	0.62	403	7	400	9	381	48	**106**
a98	7642	269	16	0.21	473	0.05608	2.0	0.66634	4.6	0.08618	4.1	0.44	352	7	518	19	1342	80	26
a99	3812	162	10	0.29	971	0.06005	1.7	0.55490	3.4	0.06702	2.9	0.51	376	6	448	12	838	61	45
a100	5363	220	18	1.08	1023	0.06189	1.9	0.54508	5.8	0.06388	5.5	0.33	387	7	442	21	737	116	52
a101	10697	532	30	0.17	5007	0.05887	1.9	0.43964	2.4	0.05416	1.5	0.77	369	7	370	7	378	34	**98**
a102	17537	917	48	0.16	32162	0.05350	2.4	0.40510	3.3	0.05492	2.3	0.73	336	8	345	10	409	51	82
a103	10770	532	30	0.42	8537	0.05546	2.7	0.42786	3.8	0.05595	2.7	0.71	348	9	362	12	450	60	77
a104	8273	370	22	0.25	15264	0.05764	1.8	0.43440	2.7	0.05466	2.0	0.67	361	6	366	8	399	44	**91**
a105	9175	464	26	0.14	12277	0.05778	1.7	0.43294	2.9	0.05434	2.3	0.60	362	6	365	9	385	51	**94**
a106	14936	721	39	0.12	6566	0.05681	1.7	0.42773	2.2	0.05461	1.3	0.81	356	6	362	7	396	29	90
a107	12394	613	34	0.14	22986	0.05704	1.7	0.42761	2.5	0.05437	1.8	0.68	358	6	361	8	386	40	**93**
a108	9294	457	27	0.24	6087	0.05867	1.8	0.43686	3.2	0.05400	2.6	0.56	368	6	368	10	371	59	**99**
a109	10657	526	30	0.17	19774	0.05789	1.9	0.43478	2.9	0.05447	2.2	0.65	363	7	367	9	390	50	**93**
a110	14554	272	43	0.84	22323	0.13068	2.0	1.18491	2.6	0.06576	1.6	0.78	792	15	794	14	799	33	**99**
a111	15136	577	34	0.19	841	0.05701	1.9	0.55574	3.7	0.07069	3.2	0.51	357	6	449	13	949	65	38
a112	6804	329	19	0.16	12702	0.05859	2.1	0.43581	3.1	0.05394	2.3	0.67	367	7	367	10	369	52	**100**
a113	2285	113	7	0.27	4245	0.05684	2.0	0.42634	4.1	0.05440	3.6	0.49	356	7	361	13	388	81	**92**
a114	25938	2222	96	0.11	2574	0.03652	2.9	0.31521	3.4	0.06260	1.6	0.87	231	7	278	8	695	35	33
a115	29237	470	41	0.26	129	0.06758	1.9	1.43859	3.3	0.15439	2.6	0.59	422	8	905	20	2395	45	18
a116	11431	573	34	0.28	20422	0.05758	1.8	0.43323	2.5	0.05457	1.8	0.72	361	6	365	8	395	39	**91**
a117	#DIV/0!	#DIV/0!	#DIV/0!	#DIV/0!	#DIV/0!	0.00000	######	#DIV/0!	#DIV/0!	#DIV/0!	######	######	0	#####	#VALUE!	#####	######	######	######
a118	12925	507	33	0.63	697	0.05590	1.9	0.50642	5.0	0.06571	4.7	0.39	351	7	416	17	797	98	44
a119	2377	111	8	0.70	4228	0.05860	2.0	0.45801	3.8	0.05668	3.2	0.53	367	7	383	12	479	71	77
a120	14273	758	42	0.38	7960	0.05635	1.8	0.43383	2.4	0.05584	1.7	0.73	353	6	366	8	446	37	79
a121	9757	417	30	0.88	687	0.05823	2.1	0.47940	4.6	0.05971	4.1	0.45	365	7	398	15	593	88	62
a122	11780	517	38	0.60	6278	0.06310	1.9	0.49889	3.9	0.05734	3.4	0.49	394	7	411	13	505	74	78
a123	12059	813	37	0.20	3387	0.03936	3.5	0.32256	5.7	0.05943	4.5	0.61	249	8	284	14	583	98	43
a124	11807	585	32	0.19	2830	0.05549	2.6	0.43990	3.8	0.05749	2.8	0.69	348	9	370	12	511	60	68
a125	32010	1527	85	0.26	1418	0.05584	1.8	0.49796	2.8	0.06468	2.0	0.67	350	6	410	9	764	43	46
a126	12080	542	31	0.56	866	0.05219	2.0	0.50576	3.9	0.07028	3.3	0.52	328	6	416	13	937	68	35
a127	11639	551	35	0.42	8285	0.05943	2.1	0.45770	2.6	0.05586	1.5	0.82	372	8	383	8	447	33	83
a128	12241	648	34	0.18	7207	0.05491	1.9	0.42177	3.8	0.05571	3.3	0.50	345	6	357	11	441	73	78
a129	9011	657	38	0.39	1456	0.05903	2.2	0.52682	6.1	0.06473	5.7	0.36	370	8	430	22	766	120	48
a130	21587	980	62	0.42	2307	0.05920	1.8	0.44848	2.4	0.05494	1.6	0.75	371	6	376	7	410	35	**90**
a131	7446	351	19	0.22	4046	0.05444	2.0	0.42036	2.7	0.05600	1.9	0.72	342	7	356	8	452	42	76
a132	9763	479	26	0.25	17013	0.05608	3.3	0.44750	4.1	0.05788	2.5	0.80	352	11	376	13	525	54	67
a133	17820	443	51	0.41	5092	0.10797	2.1	0.91524	2.5	0.06148	1.5	0.81	661	13	660	12	656	32	**101**
a134	#DIV/0!	#DIV/0!	#DIV/0!	#DIV/0!	#DIV/0!	0.00000	######	#DIV/0!	#DIV/0!	#DIV/0!	######	######	0	#####	#VALUE!	#####	######	######	######
a135	8642	302	30	1.00	2008	0.09302	3.3	0.86699	5.0	0.06760	3.8	0.66	573	18	634	24	856	78	67
a136	#DIV/0!	#DIV/0!	#DIV/0!	#DIV/0!	#DIV/0!	0.00000	######	#DIV/0!	#DIV/0!	#DIV/0!	######	######	0	#####	#VALUE!	#####	######	######	######
a137	10776	537	30	0.13	20059	0.05890	2.0	0.44070	2.8	0.05427	2.0	0.72	369	7	371	9	382	44	**97**
a138	17032	909	48	0.11	31574	0.05589	1.7	0.41886	2.7	0.05436	2.1	0.62	351	6	355	8	386	48	**91**
a139	5877	309	17	0.14	10949	0.05666	1.8	0.42516	3.4	0.05442	2.9	0.53	355	6	360	10	389	65	**91**

Sample PSC56_1125.9
Amostra PSC56_1125.9

Number	$^{207}Pb^{a}$ (cps)	U^{b} (ppm)	Pb^{b} (ppm)	$\frac{Th^{b}}{U}$	$\frac{^{206}Pb}{^{204}Pb}$	$\frac{^{206}Pb^{c}}{^{238}U}$	2 σ %	$\frac{^{207}Pb^{c}}{^{235}U}$	2 σ %	$\frac{^{207}Pb^{c}}{^{206}Pb}$	2 σ %	rho^{d}	$\frac{^{206}Pb}{^{238}U}$	2 σ (Ma)	$\frac{^{207}Pb}{^{235}U}$	2 σ (Ma)	$\frac{^{207}Pb}{^{206}Pb}$	2 σ (Ma)	conc %
A-6	9816	508	28	0.15	0	0.05591	3.3	0.41190	4.6	0.05345	3.1	0.73	351	11	350	13	347	70	**101**
A-7	7132	344	19	0.49	0	0.05598	3.7	0.45270	6.0	0.05867	4.7	0.62	351	13	379	19	554	102	63
A-8	6169	318	17	0.20	0	0.05563	3.9	0.40890	5.3	0.05333	3.6	0.74	349	13	348	16	342	81	**102**
A-9	3826	189	12	0.77	1	0.06231	3.8	0.47110	5.6	0.05485	4.2	0.67	390	14	392	18	406	93	**96**
A-10	5381	227	12	3.06	0	0.05483	3.5	0.49970	6.0	0.06611	4.9	0.57	344	12	412	20	809	103	43
A-11	4941	245	14	0.24	0	0.05965	3.6	0.45020	5.4	0.05476	4.0	0.66	373	13	377	17	402	90	**93**
A-12	2756	124	7	0.78	1	0.05601	3.8	0.44180	7.8	0.05723	6.8	0.49	351	13	372	24	500	150	70
A-13	4263	122	7	1.09	3	0.06058	3.8	0.53880	13.3	0.06452	12.7	0.29	379	14	438	47	758	269	50
A-14	732	36	2	0.70	1	0.06008	5.0	0.44760	18.0	0.05406	17.3	0.27	376	18	376	57	373	390	**101**
A-15	11805	442	24	0.48	3	0.05549	3.8	0.48830	6.2	0.06384	5.0	0.60	348	13	404	21	736	105	47
A-16	2010	93	6	2.13	b.d.	0.06189	3.9	0.96170	5.4	0.11270	3.8	0.71	387	15	684	27	1843	69	21
A-17	1193	52	3	1.03	1	0.06006	4.5	0.44530	13.5	0.05379	12.7	0.33	376	16	374	42	362	287	**104**
A-18	1538	65	4	1.06	1	0.05987	4.3	0.44700	9.7	0.05417	8.6	0.45	375	16	375	30	377	195	**99**
A-19	1710	88	6	1.77	b.d.	0.06329	4.2	1.04600	6.4	0.11990	4.9	0.65	396	16	727	33	1954	87	20
A-20	5091	203	10	1.03	1	0.04937	3.4	0.51120	8.0	0.07511	7.2	0.43	311	10	419	27	1071	145	29
A-21	7998	401	20	0.56	1	0.04970	4.2	0.38390	7.9	0.05603	6.8	0.52	313	13	330	22	453	150	69
A-22	9246	508	28	0.14	0	0.05516	3.5	0.40680	6.0	0.05350	4.9	0.58	346	12	347	18	349	112	**99**
A-23	3777	174	10	2.16	1	0.06069	3.4	0.48720	6.3	0.05824	5.3	0.54	380	13	403	21	538	116	71
A-24	3831	179	7	1.96	3	0.03816	3.6	0.33640	13.0	0.06396	12.5	0.28	241	9	294	33	740	264	33
A-25	6660	322	19	0.24	0	0.05905	3.2	0.46170	5.0	0.05671	3.8	0.65	370	12	385	16	480	83	77
A-31	8679	457	24	0.17	0	0.05421	3.4	0.40270	5.5	0.05390	4.3	0.62	340	11	344	16	366	97	**93**
A-32	2096	77	5	2.42	1	0.06254	4.1	0.59830	9.5	0.06941	8.6	0.43	391	16	476	36	910	176	43
A-33	6492	317	16	0.38	0	0.05154	3.5	0.40810	6.0	0.05744	4.8	0.59	324	11	347	18	508	106	64
A-34	9050	471	24	0.33	0	0.05236	3.6	0.39870	4.8	0.05525	3.2	0.74	329	11	341	14	422	72	78
A-35	2360	123	8	2.10	b.d.	0.06077	4.0	0.67500	7.5	0.08059	6.4	0.53	380	15	524	31	1211	125	31
A-36	13191	661	34	0.49	1	0.05225	3.3	0.39310	6.4	0.05458	5.4	0.52	328	11	337	18	394	122	83
A-37	5809	326	19	0.37	0	0.05916	3.9	0.44320	8.1	0.05435	7.1	0.49	371	14	373	25	385	159	**96**
A-38	1786	86	5	0.86	1	0.05948	4.1	0.44460	9.4	0.05423	8.4	0.43	372	15	374	29	380	190	**98**
A-39	2082	97	6	1.06	1	0.06187	4.4	0.46610	11.4	0.05465	10.5	0.39	387	17	388	37	397	235	**97**
A-40	2481	114	7	2.41	b.d.	0.06156	4.2	0.83130	5.7	0.09797	3.9	0.74	385	16	614	26	1585	72	24
A-41	2414	117	6	1.53	3	0.05402	5.5	0.76380	7.8	0.10260	5.5	0.71	339	18	576	34	1671	102	20
A-42	11439	529	27	4.45	2	0.05151	5.8	0.52570	13.9	0.07404	12.6	0.42	324	18	429	48	1042	254	31
A-43	2848	63	3	0.82	11	0.04562	4.7	0.35310	32.4	0.05615	32.1	0.14	288	13	307	86	458	711	63
A-44	26188	423	28	16.48	4	0.06224	7.4	1.26800	26.8	0.14780	25.7	0.28	389	28	832	152	2320	441	17
A-45	5682	219	14	1.54	1	0.06259	3.7	0.61910	7.1	0.07176	6.0	0.53	391	14	489	28	979	123	40
A-46	17593	502	23	0.35	4	0.04679	3.9	0.46230	7.6	0.07168	6.5	0.52	295	11	386	24	976	133	30
A-47	8161	424	23	0.10	0	0.05477	3.8	0.40720	5.2	0.05394	3.6	0.73	344	13	347	15	368	81	**93**
A-48	1565	80	6	1.33	b.d.	0.06819	5.3	1.29900	12.6	0.13820	11.4	0.42	425	22	845	72	2204	198	19
A-49	999	51	3	1.06	1	0.05720	4.1	0.42760	10.5	0.05423	9.7	0.39	359	14	361	32	380	218	**94**
A-50	5556	267	15	0.31	0	0.05807	4.0	0.43640	6.4	0.05453	5.0	0.62	364	14	368	20	392	112	**93**
A-57	2704	132	7	2.35	0	0.05686	3.9	0.42250	7.0	0.05390	5.9	0.55	356	14	358	21	366	132	**97**
A-58	1861	159	9	3.15	2	0.05834	4.0	0.44650	13.7	0.05552	13.1	0.29	366	14	375	43	433	292	84
A-59	7248	368	21	0.21	0	0.05769	3.7	0.42900	5.8	0.05395	4.5	0.63	362	13	362	18	368	101	**98**
A-60	9667	419	23	0.13	1	0.05591	3.6	0.41260	6.4	0.05354	5.3	0.56	351	12	351	19	351	121	**100**
A-61	17980	503	28	0.45	5	0.05604	3.4	0.49980	6.7	0.06470	5.8	0.51	352	12	412	23	764	122	46
A-62	1180	60	3	0.82	1	0.05582	3.8	0.41370	10.2	0.05377	9.4	0.38	350	13	352	30	361	212	**97**
A-64	8903	483	26	0.17	0	0.05416	3.4	0.39840	5.6	0.05336	4.4	0.61	340	11	340	16	344	100	**99**
A-65	5699	270	15	1.38	0	0.05424	3.4	0.45060	4.8	0.06028	3.3	0.72	340	11	378	15	613	71	56
A-67	5919	275	13	0.38	2	0.04780	4.0	0.44380	7.2	0.06736	6.0	0.55	301	12	373	23	848	125	35
A-68	2384	184	7	1.66	1	0.03795	4.1	0.53310	9.0	0.10190	8.1	0.45	240	10	434	32	1658	149	14
A-69	3109	155	9	1.17	b.d.	0.05990	3.9	0.73810	5.3	0.08940	3.6	0.74	375	14	561	23	1412	69	27
A-70	3879	194	10	0.35	0	0.05459	3.8	0.40710	5.7	0.05410	4.3	0.66	343	13	347	17	374	97	**92**
A-71	6260	489	28	0.88	2	0.05829	3.6	0.43890	7.4	0.05462	6.5	0.48	365	13	369	23	396	146	**92**

Sample PSC56_1125.9 (cont.)
Amostra PSC56_1125.9 (cont.)

Number	^{207}Pb[a] (cps)	U[b] (ppm)	Pb[b] (ppm)	Th[b] U	$^{206}Pb/^{204}Pb$	$^{206}Pb^{c}/^{238}U$	2 σ %	$^{207}Pb^{c}/^{235}U$	2 σ %	$^{207}Pb^{c}/^{206}Pb$	2 σ %	rho[d]	$^{206}Pb/^{238}U$	2 σ (Ma)	$^{207}Pb/^{235}U$	2 σ (Ma)	$^{207}Pb/^{206}Pb$	2 σ (Ma)	conc %
A-72	2466	119	7	1.19	0	0.06064	3.6	0.45180	8.5	0.05406	7.8	0.42	380	13	379	27	373	175	**102**
A-73	5909	290	16	0.12	0	0.05664	3.5	0.42110	5.4	0.05394	4.1	0.64	355	12	357	16	368	93	**96**
A-74	2557	119	7	1.76	1	0.06388	4.0	0.49070	8.0	0.05573	6.9	0.50	399	15	405	27	441	153	**91**
A-75	6940	324	17	1.82	0	0.05220	3.8	0.45820	5.6	0.06368	4.1	0.68	328	12	383	18	730	88	45
A-81	8567	446	25	0.49	0	0.05618	3.6	0.41260	6.2	0.05328	5.1	0.58	352	12	351	18	340	115	**104**
A-82	1545	74	4	1.44	1	0.05551	4.8	0.40900	11.1	0.05345	10.0	0.44	348	16	348	33	347	226	**100**
A-83	9226	416	20	1.48	0	0.04873	3.7	0.53600	5.7	0.07980	4.4	0.64	307	11	436	20	1191	87	26
A-85	4291	387	22	0.50	1	0.05772	4.0	0.42250	7.9	0.05310	6.9	0.50	362	14	358	24	333	155	**109**
A-86	1907	83	5	1.21	1	0.05904	4.3	0.44550	11.4	0.05474	10.6	0.38	370	15	374	36	401	237	**92**
A-87	12828	689	38	0.22	1	0.05556	3.7	0.40820	5.3	0.05330	3.8	0.69	349	12	348	16	341	86	**102**
A-88	3905	170	10	0.57	2	0.06044	3.8	0.50440	7.9	0.06055	6.9	0.48	378	14	415	27	623	149	61
A-89	6536	322	19	0.11	0	0.05842	3.7	0.43850	5.8	0.05445	4.5	0.63	366	13	369	18	389	101	**94**
A-90	2593	127	7	2.19	1	0.05703	3.9	0.42530	8.9	0.05411	8.0	0.44	358	14	360	27	375	180	**95**
A-91	10603	522	26	0.46	0	0.05027	3.6	0.45170	5.0	0.06520	3.5	0.72	316	11	378	16	780	73	41
A-92	1575	75	4	1.67	1	0.05815	4.3	0.43640	13.5	0.05445	12.8	0.32	364	15	368	42	389	288	**94**
A-93	11075	121	4	0.61	7	0.03088	14.0	0.78840	33.6	0.18520	30.6	0.42	196	27	590	150	2700	505	7
A-94	1737	87	5	0.71	1	0.06126	3.9	0.46110	8.4	0.05460	7.4	0.47	383	15	385	27	395	165	**97**
A-95	6847	346	20	0.13	0	0.05723	3.4	0.44500	5.5	0.05642	4.4	0.61	359	12	374	17	468	98	77
A-96	5629	387	15	1.23	b.d.	0.03769	6.9	0.69270	28.7	0.13330	27.9	0.24	238	16	534	119	2142	488	11
A-97	5111	189	12	0.83	2	0.06212	3.8	0.60700	12.1	0.07089	11.5	0.31	388	14	482	46	954	235	41
A-98	2494	121	7	1.98	1	0.06016	3.6	0.44900	8.2	0.05414	7.4	0.44	377	13	377	26	376	166	**100**
A-99	576	25	1	0.74	3	0.05894	4.6	0.46890	16.5	0.05772	15.8	0.28	369	17	390	53	518	348	71
A-100	11065	536	29	0.29	1	0.05445	3.5	0.44550	6.8	0.05936	5.9	0.51	342	12	374	21	580	128	59
A-106	12404	666	35	0.47	0	0.05351	3.5	0.40620	4.4	0.05508	2.7	0.79	336	11	346	13	415	60	81
A-107	2128	103	6	1.49	1	0.05732	4.0	0.42660	12.5	0.05399	11.8	0.32	359	14	361	38	370	266	**97**
A-108	2374	109	6	1.99	1	0.05963	3.4	0.44290	9.3	0.05388	8.6	0.37	373	12	372	29	366	194	**102**
A-109	10460	413	24	6.37	0	0.05701	3.3	0.55680	5.4	0.07086	4.2	0.62	357	12	449	20	953	87	38
A-110	1696	66	4	0.93	3	0.05491	4.3	0.40250	13.9	0.05319	13.3	0.31	345	14	343	41	336	301	**103**
A-111	8111	443	24	0.45	1	0.05477	4.2	0.40650	8.0	0.05385	6.8	0.52	344	14	346	23	364	154	**94**
A-112	1136	53	3	0.94	1	0.06177	4.6	0.46780	15.4	0.05494	14.7	0.30	386	17	390	50	409	329	**94**
A-113	7046	381	21	0.12	0	0.05491	3.7	0.40290	6.4	0.05324	5.2	0.57	345	12	344	19	338	119	**102**
A-114	3648	186	8	1.50	8	0.04377	4.6	0.48200	14.0	0.07990	13.2	0.33	276	12	399	46	1194	260	23
A-115	7169	326	18	0.24	1	0.05727	3.7	0.47030	8.2	0.05957	7.3	0.45	359	13	391	27	587	159	61
A-116	5689	552	32	0.30	0	0.05855	3.5	0.43800	7.9	0.05427	7.1	0.44	367	12	369	25	382	161	**96**
A-117	3674	195	12	0.93	0	0.06110	4.5	0.45500	10.6	0.05402	9.6	0.42	382	17	381	34	371	217	**103**
A-118	6837	360	21	0.11	0	0.05909	3.5	0.44550	5.2	0.05470	3.8	0.67	370	12	374	16	399	86	**93**
A-119	1216	56	3	0.87	2	0.05970	4.1	0.45250	14.8	0.05498	14.3	0.27	374	15	379	47	411	319	**91**
A-120	10458	411	23	0.33	1	0.05469	3.5	0.56100	5.7	0.07441	4.6	0.61	343	12	452	21	1052	92	33
A-121	2570	117	7	1.34	1	0.05662	4.0	0.44850	10.2	0.05746	9.3	0.39	355	14	376	32	509	206	70
A-122	5950	324	18	0.12	0	0.05800	3.6	0.43370	5.5	0.05424	4.2	0.65	363	13	366	17	380	94	**96**
A-123	2272	208	13	0.70	0	0.06288	3.7	0.47170	6.8	0.05442	5.7	0.54	393	14	392	22	388	129	**101**
A-124	3843	291	18	0.67	2	0.06307	3.7	0.51970	9.3	0.05978	8.5	0.40	394	14	425	32	595	184	66
A-125	1426	134	9	1.71	b.d.	0.06441	4.3	1.31700	6.8	0.14840	5.3	0.63	402	17	853	39	2327	91	17
A-131	5421	269	16	1.13	1	0.05914	3.7	0.47310	6.8	0.05803	5.7	0.54	370	13	393	22	530	125	70
A-132	4485	220	14	1.72	0	0.06257	3.6	0.48550	6.7	0.05629	5.6	0.54	391	14	402	22	463	124	85
A-133	3776	191	11	0.62	0	0.05797	3.6	0.43340	6.0	0.05423	4.8	0.59	363	13	366	18	380	109	**96**
A-134	11994	659	33	0.08	0	0.05161	3.3	0.38690	4.2	0.05439	2.6	0.79	324	10	332	12	387	59	84
A-135	3619	339	22	1.92	b.d.	0.06328	4.6	0.79170	7.5	0.09076	5.9	0.62	396	18	592	34	1441	113	27
A-136	1220	63	4	1.32	b.d.	0.06018	4.1	1.08900	6.0	0.13130	4.3	0.69	377	15	748	32	2115	76	18
A-138	6355	299	15	0.20	0	0.05181	3.7	0.43610	6.2	0.06107	5.0	0.60	326	12	368	19	641	108	51
A-139	8011	343	19	0.18	1	0.05488	5.8	0.40440	7.8	0.05345	5.2	0.75	344	20	345	23	347	118	**99**
A-140	6323	313	18	0.26	0	0.05891	3.8	0.46950	5.9	0.05782	4.5	0.65	369	14	391	19	522	99	71
A-141	5998	313	19	0.93	0	0.06073	3.4	0.46230	5.8	0.05523	4.7	0.59	380	13	386	19	421	105	**90**
A-142	4986	178	11	0.70	8	0.06379	4.2	0.63340	12.3	0.07203	11.5	0.34	399	16	498	48	986	234	40
A-143	10332	456	25	0.19	1	0.05478	3.5	0.40400	6.9	0.05350	5.9	0.51	344	12	345	20	350	133	**98**
A-144	9072	502	25	0.25	0	0.05127	3.7	0.39070	4.6	0.05528	2.7	0.80	322	12	335	13	423	61	76
A-145	5659	217	12	1.19	2	0.05630	4.0	0.49590	10.0	0.06391	9.2	0.40	353	14	409	34	738	194	48
A-146	1064	70	4	0.80	3	0.05445	4.7	0.44980	23.0	0.05992	22.5	0.20	342	16	377	72	600	487	57
A-147	26260	240	14	1.24	37	0.05910	5.3	0.68190	20.0	0.08371	19.3	0.27	370	19	528	82	1285	375	29
A-148	1674	68	4	1.55	1	0.06025	4.2	0.53880	13.3	0.06488	12.6	0.31	377	15	438	47	770	265	49
A-149	21389	556	31	0.44	7	0.05565	3.8	0.49140	8.0	0.06405	7.1	0.47	349	13	406	27	743	150	47
A-150	12300	734	39	0.34	1	0.05411	4.2	0.39500	7.9	0.05296	6.7	0.53	340	14	338	23	326	152	**104**
A-156	6645	363	20	0.19	0	0.05709	3.5	0.41890	5.0	0.05322	3.6	0.69	358	12	355	15	338	83	**106**
A-157	7507	326	18	0.53	2	0.05735	3.5	0.44880	7.8	0.05677	7.0	0.45	359	12	376	25	482	155	75
A-158	3144	236	14	1.25	2	0.06084	4.1	0.52780	10.6	0.06294	9.7	0.39	381	15	430	37	706	207	54
A-159	8194	378	19	0.42	1	0.05038	4.0	0.41120	8.2	0.05921	7.1	0.49	317	12	350	24	574	155	55
A-160	6518	356	20	0.34	0	0.05630	3.6	0.41310	6.1	0.05323	4.9	0.60	353	12	351	18	338	110	**105**
A-161	10010	586	31	0.13	0	0.05316	3.2	0.39460	4.1	0.05386	2.5	0.78	334	10	338	12	365	57	**92**
A-162	1123	101	6	1.30	1	0.06071	3.5	0.47620	11.3	0.05691	10.8	0.31	380	13	395	37	487	238	78

[a] within-run background-corrected mean ^{207}Pb signal in counts per second
[b] U and Pb content and Th/U ratio were calculated relative to GJ-1 and are accurate to approximately 10%.
[c] corrected for background, mass bias, laser induced U-Pb fractionation and common Pb (if detectable, see analytical method) using Stacey and Kramers (1975) model Pb composition. $^{207}Pb/^{235}U$ calculated using $^{207}Pb/^{206}Pb/(^{238}U/^{206}Pb \times 1/137.88)$. Errors are propagated by quadratic addition of within-run errors (2SE) and the reproducibility of GJ-1 (2SD).
[d] Rho is the error correlation defined as $err^{206}Pb/^{238}U/err^{207}Pb/^{235}U$.

[a] média de fundo corrigida durante a medição de sinal ^{207}Pb em contagens por segundo.
[b] o conteúdo U e Pb e a razão Th/U foram calculados relativamente ao padrão GJ-1 e são precisos a aproximadamente 10%.
[c] corrigido para fundo, erros de massa, fracionamento U-Pb induzido pelo laser e Pb comum (se for detetável, ver método analítico) usando o modelo de composição de Pb de Stacey e Kramers (1975); $^{207}U/^{235}Pb$ calculado usando $^{207}Pb/^{206}Pb/(^{238}U/^{206}Pb$ x 1/137.88); os erros são propagados for adição quadrática de erros durante a leitura (2SE) e a reprodutibilidade do GJ-1 (2SD).
[d] Rho é o erro de correlação definido como $err^{206}Pb/^{238}U/err^{207}Pb/^{235}U$.